



## Article

# Tribological and Mechanical Properties of the Nanostructured Superlattice Coatings with Respect to Surface Texture

Ernests Jansons <sup>1,\*</sup>, Janis Lungevics <sup>1</sup>, Uldis Kandars <sup>1</sup>, Armands Leitans <sup>1</sup>, Guna Cīvica <sup>1</sup>, Oskars Linins <sup>1</sup>, Karlis Kundzins <sup>1,2</sup> and Irina Boiko <sup>1</sup>

<sup>1</sup> Institute of Mechanics and Mechanical Engineering, Faculty of Mechanical Engineering, Transport and Aeronautics, Riga Technical University, LV-1048 Riga, Latvia

<sup>2</sup> Institute of Solid State Physics, University of Latvia, LV-1586 Riga, Latvia

\* Correspondence: ernests.jansons\_1@rtu.lv

**Abstract:** Ceramic Nanostructured Superlattice Coatings (NSC) have broad applicability to improve the parts' and assemblies' tribological and mechanical properties for the needs of the automotive and aerospace industries. Improving the material properties using nanocoatings for such a widely used material as, for example, bearing steel 100Cr6 makes it possible to improve the service life of machine parts. In this paper, the correlation dependence between tribological and mechanical properties of the NSC and its surface texture are considered to determine how much surface texture will affect the tribological performance of the coated workpieces, as well as the measuring and evaluation procedure of the nanocoatings, are presented. Three different NSC described by a general empirical formula  $\{\text{TiMe1Me2-CN/TiAlSi-N}\}_n$  and based on the modified carbonitride/nitride non-stoichiometric chemical composition were created, and their tribological and mechanical properties measured and analyzed in the context with surface texture. NSC deposited by the advanced PVD (Physical vapor deposition) technique demonstrated significantly higher wear resistance (up to 28 times), reasonably lower friction coefficient (CoF) (up to 4 times), and significantly higher hardness of the coated workpieces (up to 7 times) versus substrate material. A strong correlation between the steady-state dry sliding friction, CoF, and the amplitude and functional surface texture parameters of tribo-track were observed. The first results of the initiated research regarding the correlation analysis of the tribological and mechanical properties, on the one hand, and surface texture, on the other hand, of the NSC are reported here.

**Keywords:** surface texture; nanostructured carbonitride coatings; microhardness; wear; friction coefficient; tribology



**Citation:** Jansons, E.; Lungevics, J.; Kandars, U.; Leitans, A.; Cīvica, G.; Linins, O.; Kundzins, K.; Boiko, I. Tribological and Mechanical Properties of the Nanostructured Superlattice Coatings with Respect to Surface Texture. *Lubricants* **2022**, *10*, 285. <https://doi.org/10.3390/lubricants10110285>

Received: 12 October 2022

Accepted: 26 October 2022

Published: 28 October 2022

**Publisher's Note:** MDPI stays neutral with regard to jurisdictional claims in published maps and institutional affiliations.



**Copyright:** © 2022 by the authors. Licensee MDPI, Basel, Switzerland. This article is an open access article distributed under the terms and conditions of the Creative Commons Attribution (CC BY) license (<https://creativecommons.org/licenses/by/4.0/>).

## 1. Introduction

Solutions have long been sought to improve material properties such as abrasion resistance, hardness, and friction. Improved material properties extend the service life of specific units and, consequently, the whole machine, reducing the need for new parts, repairs, and thus unnecessary energy consumption. Methods to improve machine parts and assemblies have varied from different heat treatments [1–4] to applying coatings with different complexities [5–8].

Different nanocoatings are used to improve the base material's characteristics of traditional bulk materials in such sectors as electronic components, aeronautics, medical equipment, industrial manufacturing, transportation, and others. It is well known that nanocoatings can be deposited by different methods [9]. Among them, PVD technologies are one of the most promising methods because they allow obtaining highly dense nanostructured ceramic coatings with smooth surfaces, i.e., low RMS (Root mean square) value, thus increasing the tribological properties of the material. The advanced PVD technique has been used in this research work, denoted here as the High-Power Ion-Plasma

Magnetron Sputtering (HiPIPMS). To overcome multiple tribological and mechanical limitations mentioned by a few researchers [10–14], a novel approach based on modified 3-phase non-stoichiometric carbonitride/nitride films in this study will be used. NSC based on carbonitride/nitride constituents (denoted here {-CN/-N}) would theoretically be harder even than diamond-type coatings if they could be deposited in the same structure as  $\text{Si}_3\text{N}_4$ , i.e.,  $\text{C}_3\text{N}_4$ . Some specific carbonitride/nitride coatings produced and reported up to now have shown extreme elastic and tribological properties [15,16] combined with relatively high hardness values in the range of about 20–60 GPa. Therefore, the research strategy was based on modified non-stoichiometric NSC based on  $\{\text{TiMe}_1\text{Me}_2\text{-CN/TiAlSi-N}\}_n$  where ‘ $\text{Me}_1$  and  $\text{Me}_2$ ’ denote alloying metallic additives as Cr, Nb, W, and Zr, but subscript ‘ $n$ ’ indicates a number of periods within the NSC containing alternating {carbonitride/nitride} sublayers. Thus, the goal was to achieve a novel solution to sufficiently reduce or even eliminate well-known disadvantages of the hard pure carbon-based or nitride-based coatings, i.e., inherent compressive macro-stresses, not-good-enough adhesion to steel workpieces, and reduced thermal stability due to the denitrification of coatings.

Another aspect is the quality of the working surface of the parts, its complete characterization, and its impact on the tribological and mechanical properties. Given the current state of technology, it is already known that 3D texture measurements should be used instead of 2D for more accurate surface characterization. Wang et al. [17] presented a study on surface roughness, which was evaluated using a 2D and 3D profiling approach. These results proved that 3D surface texture parameters such as  $S_a$  (Arithmetical mean height) and  $S_q$  (Root mean square height) are more accurate in describing the surface quality than the corresponding 2D parameters— $R_a$  (Arithmetical mean height of the profile) and  $R_z$  (Maximum height of profile). Additionally, the standard error of 3D surface texture parameters is lower than that of 2D parameters. Similar results were obtained by Deleanu et al. [18] by analyzing 2D and 3D surface texture parameters for both metal and polymer blocks. The standard error for 2D surface texture parameters was more significant than for 3D parameters in all cases. Moreover, the use of focus-variation microscopy [19] to acquire 3D surface characteristics and evaluate the surface quality of laser cut edges using areal surface roughness parameters (parameters  $S_a$  and  $S_{10z}$  (height of the 10 points of the surface)) has shown the reliability of the standard 2D texture parameters is low. In one more paper [20], it was stated that the 3D approach choosing five 3D surface texture parameters, such as  $S_{ds}$  (Density of peaks),  $S_{dq}$  (Root mean square gradient),  $S_{sc}$  (Arithmetic mean summit curvature), and  $S_{dr}$  (Developed interfacial area ratio), describes operational surfaces more precisely than the 2D approach.

Several studies are known to investigate a correlation between surface texture and friction-wear characteristics. Menezes et al. [21] analyzed the effect of surface texture on hardness and friction during unidirectional sliding, concluding that the friction coefficient (CoF) predominantly depends on the hardest surface texture. It was pointed out [22] that the basic amplitude parameters commonly used to describe tribological characteristics are insufficient to determine the tribological properties of contact surfaces. Therefore, other surface topography parameters should be used to describe the tribological properties of the friction pairs. Pawlus et al. [23] performed a pervasive analysis of the functional importance of surface texture parameters, taking into account the parameters listed in ISO 25178. Pawlus concluded that most surface texture parameters are related to friction and wear; however, it is vital to know the application of friction pair. Amplitude parameters are most commonly used and are related to friction, lubrication, and wear. Skewness  $S_{sk}$  and kurtosis  $S_{ku}$  characterizes the shape of the height distribution. Negative skewness typically improves the contact of rough surfaces. The hybrid parameters are more related to the rough surfaces of the contacts. Correspondingly, the parameters related to the material ratio curve or functional parameters are also related to friction and wear, but the main problem is the selection of groups of parameters that describe the material ratio curve. Surface texture parameters to describe surfaces obtained by grinding, lapping, and electrochemical machining processes were, by importance, classified by Kacalak et al. [24].

Both the parameters listed in the standard ISO 25178 and the feature parameters introduced by the author were used, obtaining that the feature parameters S5p (Five-point peak height), S10z, and height parameters (Sp (Maximum peak height), Sv (Maximum pit height), Sa, Sq) indicate a high ability to distinguish characteristic surface features. In Zak et al. [25], the surface textures produced by different machining operations were analyzed regarding their potential functionality: the parameters Sa, Ssk (Skewness), Spk (Reduced peak height), Vmp (Peak material volume), and Vvv (Pit void volume) showed a strong correlation with fluid retention abilities and tribological properties. Jansons et al. [17] concluded that from four surface 3D surface texture parameters (Sa, Ssk, Sds, Sdq), the Sa is the most useful for ice friction surface characterization. Das et al. [26] analyzed a systematic and appropriate selection of surface roughness parameters for extruded and ground surfaces that could act as process monitoring indices. It was obtained that the 3D parameter ratio Spk/Sk can be used to define the surface lay. Another option may be a combination of skewness and kurtosis to define the shape of the profile to determine the oil retention capacity. Ratios Spk/Sk, Svk/Sk, and Spk/Svk can be used to measure load-carrying capacity.

In light of the known literature, it can be concluded that extensive work has been undertaken in recent years to find the correlation dependence between the 3D surface texture parameters and the tribological properties of the material. However, surfaces with treatment traces from machining and relatively high surface roughness are primarily analyzed (see Table 1). However, no correlation between surface texture and tribological properties has been sought for coatings with relatively small surface roughness (Sa below 0.015  $\mu\text{m}$ ).

**Table 1.** Sa values measured by different authors.

Author	Machining Process	Sa, $\mu\text{m}$
Zeng et al. [27]	Grinding, turning	0.3
Dzierwa et al. [22]	Sand blasting	3.6–4.2
Zak et al. [25]	Turning	0.2
Jansons et al. [28]	Polishing, scratching	0.015–0.2
Das et al. [26]	Extrusion, grinding	1.5–6.5
Shi et al. [29]	Grinding	0.9–3.8

The Table lists the literature sources where the Sa value could be determined.

If the correlation between the surface texture parameters of different friction pairs and the friction properties has been studied in the works of several authors, then the correlation between hardness and surface texture is considered less frequently. That may be related to the technological provision, i.e., when measuring the hardness of the material with a sufficiently high load (using the most popular methods of measuring the hardness of the material, for example, Brinell, Vickers, Rockwell), surface irregularities do not noticeably affect the measurement result. Hardness measurement methods such as microhardness and nanohardness should be used to analyze surface texture's effect on hardness.

When measuring microhardness or nanohardness, the effect of surface texture can be significant to the measurement result. Bohme et al. [30] studied microhardness measurements of stainless steel samples on a milled (Ra 125–240 nm) and polished surface (Ra 2–3 nm). Indentation measurements for the milled samples indicated a scatter of the measurement results, although the hardness should not change. If the indentation is made in a valley, the material appears harder, but if the indentation is made on a peak, it appears softer. Therefore, in order to be able to analyze the microhardness results, the surface texture must be measured at the point of indentation. The sample's surface must also be prepared as smoothly as possible for qualitative microhardness measurements. Microhardness measurements on a milled surface indicated an error of at least 40%, while the error did not exceed 8% on a polished surface.

The surface must be even smoother if the nano-indentation method is used. The thin film was deposited on a silicon wafer substrate, and cyclic nano-indentation to deter-

mine the mechanical properties of the coating on the surface (RMS 0.5 nm) was used in Plichta et al. [31] work. The surface texture significantly affected the near-surface mechanical properties, and the measured values varied up to 100% compared to the actual value depending on the surface at the measurement position. Analyzing the nanohardness of Cu/Ni multilayer structures, Kulej et al. [32] concluded that the hardness measurements results are related to the surface texture, i.e., a smoother surface provides higher nanohardness. Although some investigations concerning surface texture and micro or nanohardness have been done, the correlation between several 3D surface texture parameters and hardness measurements has not been reported yet in the known literature.

This work aims to analyze the correlation dependence between tribological and mechanical properties of the NSC and their surface texture parameters to determine how much surface texture will affect the tribological performance of the coated workpieces. This work stresses the measuring methods of the NSC and evaluation procedures of the obtained data rather than the coatings' microstructure, morphology, and other physiochemical properties.

## 2. Materials and Methods

### 2.1. Preparation of the Samples

The NSC samples were deposited onto bearing steel disk-shaped substrates ( $\varnothing 30 \times 4$  mm) made of 100Cr6 using the HiPIPMS technique. The HiPIPMS was implemented on the Thin Film Modular Deposition System (TF-MDS) [33,34]. The TF-MDS had four cross-configured workstations equipped with magnetron sputtering devices (MSD), up to 8 MSDs altogether (Figure 1). The cross-configuration of the workstations on the circumference inside the vacuum chamber allows numerous specific combinations of monolithic and mosaic-type magnetron sputtering targets (MST) mounted onto MSDs depending on the requested chemical composition of the NSC. MSDs were operated in the effective crossed-field unbalanced magnetron sputtering ion-plasma mode, providing a highly ionized plasma environment in the whole space between the MST and substrate-holder. Thus, immersed sputtering plasma mode was realized nearby of both surfaces of the MST and Substrate. The plasma environment within the MST-substrate space enhanced the chemical reactivity of the sputtered particles condensed on the substrate and activated carbonitride/nitride film growth. Sputter cleaning of the substrates was performed prior to film deposition by a collimated linear ion beam device which was also used for film growing activation and resputtering weakly accommodated particles during the film deposition process.

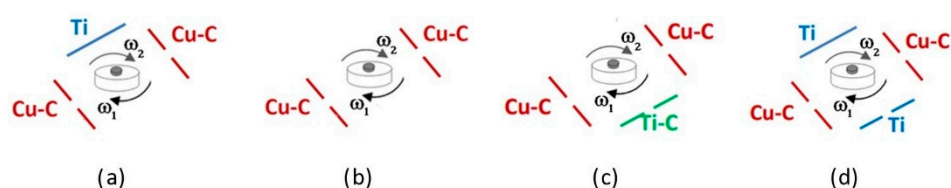


**Figure 1.** Schematic of the Thin Film Modular Deposition System (TF-MDS) with four workstations equipped with up to  $8 \times$  MSDs. Variations for the specific PVD process, for instance, (a)  $4 \times$  mosaic-type MST of Cu-C and  $1 \times$  monolithic MST of Ti; (b)  $4 \times$  mosaic-type MST of Cu-C; (c)  $4 \times$  mosaic-type MST of Cu-C and  $2 \times$  mosaic-type MST of Cu-C; (d)  $4 \times$  mosaic-type MST of Cu-C and  $1 \times + 2 \times$  monolithic MST of Ti.

The PVD technologies applied for obtaining NSC samples and their modification are based on the modern design and engineering capabilities of the deposition system TF-MDS. The modular design of TF-MDS provides the possibility of simultaneous use of up to  $8 \times$  MSDs where, in principle, each MSD can be mounted with the MST of a different material [35,36]. Therefore, the TF-MDS design allows flexibly modifying the technological parameters of the PVD process, the chemical composition of the obtained nanocomposite coating, and its physical-mechanical and electrophysical properties. For example, the material of which the MST is made and MSTs configuration in the vacuum chamber determine the structure of the coating layers and their chemical composition. In addition,

the 1D and/or 2D rotation of the sample holder carousel determines the coating density and thickness uniformity. In turn, ion-plasma discharge power on the MSDs determines the film deposition rate and nanostructure at the atomic level (see Figure 1).

The morphology of the coating structures was investigated using a scanning electron microscope (SEM) Tescan Lyra3 (Tescan, Brno, Czechia), equipped with an energy-dispersive X-ray spectrometer (EDS) Oxford Aztec (Oxford Instruments, Abingdon, UK). SEM and EDS measurements were performed using a beam-accelerating voltage of up to 30 kV and a beam current of 500 pA.

## 2.2. Tribology Tests

The tribology tests were performed to analyze the wear and friction coefficient using a ball-on-disc tribometer TRB<sup>3</sup> (CSM Instruments, Needham Heights, MA, USA) under dry friction conditions. Samples were tested using a 100Cr6 (EN 683-17) steel ball (Ø6 mm). All tests were performed at room temperature  $21 \pm 1$  °C. Experimental settings for friction and wear tests were based on recommendations in standard ISO 18535 (Diamond-like carbon films—Determination of friction and wear characteristics of Diamond-like carbon films by ball-on-disc method).

Friction tests were performed for 5000 cycles at a 3 mm tribo-track radius (100 m total distance) and 0.15 m/s linear speed. The normal load was set to 3 N.

For wear tests, the total number of cycles was increased to 1000 m total distance and 0.1 m/s linear speed. The normal load was set to 5 N. The wear track was measured in 8 positions at a constant angular distance using a SurfTest SJ-500 (Mitutoyo, Kawasaki, Japan) surface roughness tester. Wear cross-sectional area was calculated using Talymap Gold analysis software, version 4.1.1.

## 2.3. Surface Texture Measurements

A Talysurf Intra 50 (Taylor Hobson, Leicester, UK) profilometer with a 112/2009 stylus (2 µm tip diameter) was used to characterize surface texture. The total area measured was  $2 \times 2$  mm, including both the smooth part of the surface and the tribo-track part. The texture was measured from 300 profiles, with each profile line consisting of 10,000 points, for a total of 3,000,000 points per measurement.

Data post-processing was performed with Talymap Expert software, version 3.2.0. Initially, the primary surface was leveled, followed by the separation of the surface roughness and the waviness portion (see Figure 2). Smooth surface part and tribo-track part measurements were performed with a different cut-off based on the recommendations of standard ISO 25178-3. The cut-off value of 0.08 was used for the smooth surface part and 0.25 for the tribo-track surface part for all measured samples. The separated roughness was then zoomed in to the surface from the smooth or tribo-track area ( $200 \times 500$  µm), and 3D surface texture parameters were obtained.

The surface texture was measured for a total of 9 coated and for the reference sample. In total, 31 surface texture parameters (ISO 25178-2) and ratios [23,28] were considered in this work (see Table 2). Three-dimensional surface texture parameters, for various reasons, do not indicate a significant difference between the measuring sample surfaces in the given case; for example, spatial parameter Std, which depends on the surface orientation during a measurement, was not considered. Moreover, the 3D surface texture parameters that require additional necessary information for performing a correct analysis, for example, the parameter Smr, or areal material ratio, which directly depends on the level from the highest peak, and related parameters such as Smc (inverse material ratio) were not considered.



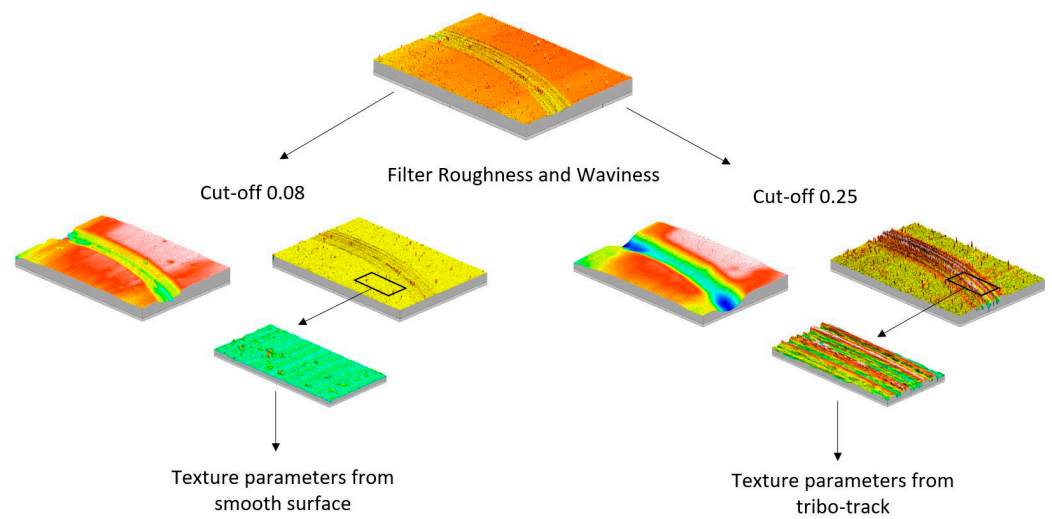


**Figure 2.** Surface texture measurement scheme. From one 3D measurement, 3D surface texture parameters are calculated for tribo-track and smooth surfaces using different cut-off values.

**Table 2.** Surface texture parameters considered.

Parameters Group	Symbol	Unit	Description
Amplitude parameters	Sa	$\mu\text{m}$	Arithmetical mean height
	Sq	$\mu\text{m}$	Root mean square height
	Sp	$\mu\text{m}$	Maximum peak height
	Sv	$\mu\text{m}$	Maximum pit height
	Ssk		S kewnness
	Sku		Kurtosis
	Sz	$\mu\text{m}$	Maximum height
	Rsm	mm	Mean profile spacing
	Rsm/Sa		Ratio of mean profile spacing to the arithmetical mean height
	Sq/Sa		Ratio of root mean square height to arithmetical mean height
Sp/Sz		Ratio of maximum peak height to the maximum height	
Spatial parameters	Sds	pks/mm <sup>2</sup>	Density of peaks
	Str		Texture aspect ratio
	Sal	mm	Autocorrelation length
	Sfd		Fractal dimension of the surface
Hybrid parameters	Sdq		Root mean square gradient
	Ssc	1/ $\mu\text{m}$	Arithmetic mean summit curvature
	Sdr	%	Developed interfacial area ratio
Functional parameters	Sk	$\mu\text{m}$	Core height
	Spk	$\mu\text{m}$	Reduced peak height
	Svk	$\mu\text{m}$	Reduced valley depth
	Sr1	%	Material ratio for peaks
	Vv	mm <sup>3</sup> /mm <sup>2</sup>	Void volume
	Vm	mm <sup>3</sup> /mm <sup>2</sup>	Material volume
	Vmp	mm <sup>3</sup> /mm <sup>2</sup>	Peak material volume
	Vmc	mm <sup>3</sup> /mm <sup>2</sup>	Core material volume
	Vvc	mm <sup>3</sup> /mm <sup>2</sup>	Core void volume
	Vvv	mm <sup>3</sup> /mm <sup>2</sup>	Valley void volume
Spk/Sk		Ratio of reduced peak height to core height	
Svk/Sk		Ratio of reduced valley depth to core height	
Spk/Svk		Ratio of reduced peak height to reduced valley depth	

In this analysis, parameters can be classified into four groups—Amplitude, Spatial, Hybrid, and Functional.

The most typical amplitude parameters which are used in surface characterization were considered. According to the literature [23,24,26,29,37,38], it is known that Sa, Sq, Sz, Sp, Sv affect surface contact, lubrication, friction, wear, as well as such parameters as Ssk, Sku, and ratios Sp/Sz, Sq/Sa, which characterize the shape of the height distribution. Sa and Sq parameters, usually used to characterize the surface texture, are not sufficient to characterize the tribological process of contacting surfaces. It was obtained that Sku and Ssk parameters showed a higher correlation with the wear process than Sa and Sq [22]. In the boundary and mixed lubrication friction regimes, parameters Ssk and Sku impact friction [39]. The pitch parameter Rsm and Rsm/Sa are included in the wear calculations [40], and it has also been observed that the friction properties on the ice can be estimated [28]. Rsm for each sample was calculated as an average from five separate profiles extracted from the measured 3D surface.

Spatial parameters Sal (Autocorrelation length) and Str (Texture aspect ratio) affect lubrication and friction [23]. The Sds parameter is an important parameter used in bearings and seals because it is related to how surfaces deform elastically and plastically under load [41]. The Sfd (Fractal dimension of the surface) parameter describes the complexity of the surface using the fractal dimension theory, thus indicating whether the surface is flat or complex, and Sfd correlates with Sds for the honed surfaces [25].

The hybrid parameters, which combine information on height and spatial parameters, Sdq and Sdr, affect surface contact, friction, and wear properties. Sdq is highly dependent on Sq; accordingly, Sdr is dependent on Sdq. The Ssc parameter is used in contact mechanics to characterize the plastic deformation affecting the wear [23].

The functional group of parameters related to the material ratio curve affects wear and friction [23]. For example, Vmc (Core material volume) is the most relevant parameter to characterize the rolling process [38], or Vvv and Vvc (Core void volume) parameters are related to valleys of the surface, which reflect lubricant storage performance [23,42]. Moreover, Vvv and Vvc correlated with the friction coefficient of a rough contact interface [29]. Parameters related to the material ratio curve were calculated using default material ratios of 10 and 80%.

#### 2.4. Microhardness Measurements

Microindentation provided information about the integrated coating hardness, including the hardness of both Coating and the Substrate. Micro-Vickers indenter HM210D (Mitutoyo, Kawasaki, Japan) with complete CNC XY sample holding stage was used for the tests. Lenses with 50× and 100× magnification were used for indentation diagonals measurements. Complete CNC control over the sample holding stage provided semi-automatic sample testing with various indentation forces and a test matrix with evenly distributed distances between indentations.

Twelve different test forces were used for each sample from 0.1–6.0 N. Information about the integrated hardness is essential to understand the whole system (Coating + Substrate) usability in tribological applications because both components play a significant role in the final performance, i.e., hard coating on too soft substrate might fracture if the substrate surface bends. Thus, finding optimal combinations of coating hardness and substrate hardness is essential.

### 3. Results and Discussion

#### 3.1. NSC Samples

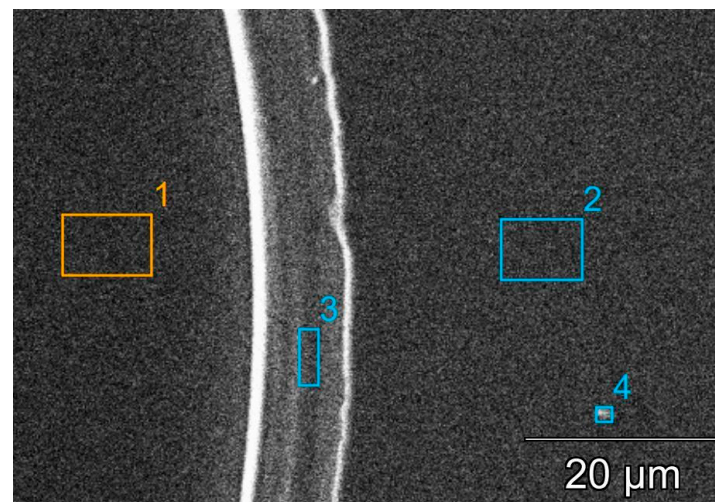
All substrates are unique, as it is impossible to prepare them with identically polished surfaces. Therefore, ten samples are considered in the study—9 of them are coated with the NSC, and one is uncoated (see Table 3). Each sample was studied tribologically and mechanically, as well as using electron microscopy and profilometry. Correlation dependence between the mechanical and tribological properties of the samples and the surface texture parameters was sought.

**Table 3.** Micromechanical parameters of the superlattice-type NSC samples based on the alternating carbonitride/nitride {TiMe-CN/TiAlSi-N} 2-sublayers spatial period.

PVD Process	Sample Label	Coating's Laminated Structure	Thickness, (nm)
NSC 1	NSC 1.1; NSC 1.2; NSC 1.3	{TiWZr-CN/TiAlSi-N} <sub>270</sub>   Ti   Substrate	~6500
NSC 2	NSC 2.1; NSC 2.2; NSC 2.3	{TiCrNb-CN/TiAlSi-N} <sub>300</sub>   Ti   Substrate	~5200
NSC 3	NSC 3.1; NSC 3.2; NSC 3.3	{Si-CN/Cr-N} <sub>230</sub>   Ti   Substrate	~5500
	Substrate	Bulk bearing steel 100Cr6, Ø30 × 4 mm	

The Calo tester (CSM Instruments, Needham, MA, USA) and KH7700 optical microscope (Hirox, Tokyo, Japan) were used to measure the thickness of the coatings. The coating thickness was measured to be greater than 5200 nm for all samples.

Four characteristic spots on the sample surface were chosen to analyze the coating's chemical composition (see Figure 3). Spot-1 is a sample surface without coating, i.e., a substrate; spot-2 as a nearby smooth surface region of the coating; spot-3 as a coating's deeper sublayers as worn tribo-tracks and/or flaked or detached coating's pieces; and finally, spot-4 as a nearby surface region of the coating having some irregularity, unlike the spot-2.

**Figure 3.** NSC 2.1 sample SEM micrograph of the sample surface showing mentioned above four spots (1-2-3-4) where EDS spectra were taken.

The elements observed in the EDS spectra exhibiting their weight and atomic content within the coating are summarized in Table 4. It is seemingly that the chemical composition of the coating affects its micromechanical and tribological properties, i.e., the overall tribological performance.



**Table 4.** Summary table of the chemical elements observed in the EDS spectrum of the NSC 1.1, NSC 2.1, NSC 3.1 samples taken from the spot-'2' on the coating's surface. The content of elements is exhibited in their atomic-%.

Sample	C	N	Al	Ti	Fe	Zr	Ag	W	Si	Cr	Nb	Hf
NSC 1.1	20.83	17.86	15.82	16.55	1.91	9.53	1.44	16.07	-	-	-	-
NSC 2.1	13.86	29.65	14.62	25.42	0.26	-	-	-	2.21	8.64	5.35	-
NSC 3.1	16.50	16.19	0.29	0.66	0.86	-	-	-	12.92	52.51	-	0.08

### 3.2. Wear and Friction Coefficient

Two different tribological experiments were performed. One characterized the wear of the Coatings, and the other the friction properties.

#### 3.2.1. Wear

The wear tests were conducted according to standard ISO 18535 as described in the materials and methods section. The wear track was measured in eight positions at a constant angular distance, and the average value of the cross-sectional area was calculated for each coating. Examples of wear profiles for three coatings are shown in Figure 4. NSC 1.1 is represented in red, and NSC 2.1 and NSC 3.1 are in green and blue colors, respectively. The gray area represents the substrate material. From the measured coating thicknesses (see Table 3), NSC 3.1 is worn to the substrate material. NSC 1.1 and 1.2 are worn to a depth of approximately 3  $\mu\text{m}$ , but NSC 2.1 is slightly wider.

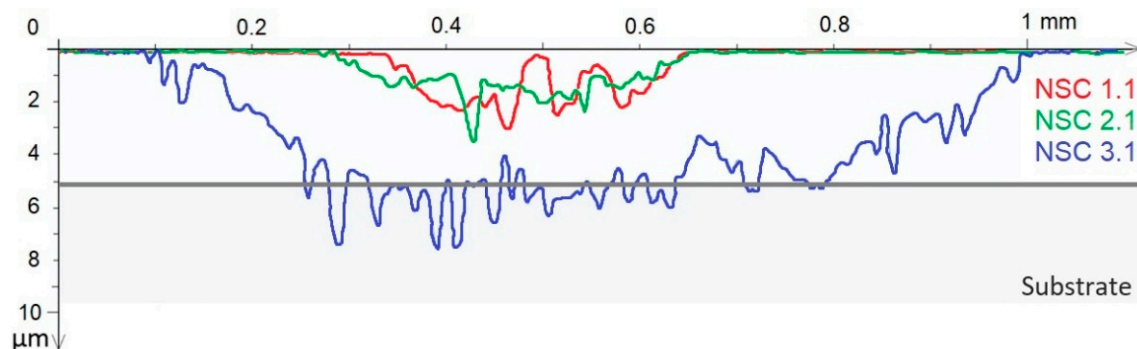


**Figure 4.** Wear cross-sectional profiles for three different coatings. NSC 1.1—red, NSC 2.1—green, NSC 3.1—blue, substrate—grey.

The wear cross-sectional area was calculated for each profile using the Talymap Gold analysis software, and the average value was calculated for each Coating and Substrate (see Table 5). The average cross-sectional area was used as the wear-describing parameter in this case. The obtained data shows that the best wear-resistant Coating is NSC 1.1, improving the wear properties about 28 times against the substrate material. The worst wear resistance was observed in NSC 3.1, with approximately three times better wear properties against the substrate material. As the wear increases, the numerical value of the standard deviation of the measurements increases. That can be explained by the fact that as the total worn area increases, the numerical value of the standard deviation also increases proportionally, as well as for a material or coating with low wear resistance, wear debris impact and separation of layers is possible in specific places, which accordingly affects the size of the wear cross-sectional area and standard deviation.

**Table 5.** Average wear cross-sectional area (Ball material—100Cr6, Total distance 1000 m, Linear velocity 0.1 m/s, Test force—5 N).

	Avg. Cross-Sectional Area, $\mu\text{m}^2$
NSC 1.1	385 $\pm$ 40
NSC 2.1	541 $\pm$ 90
NSC 3.1	3232 $\pm$ 420
Substrate	10,665 $\pm$ 1400

### 3.2.2. Friction Coefficient

The friction coefficient was measured according to the settings described in materials and methods to characterize the friction properties of the coatings. Measurements were performed on three samples for each coating and the substrate material. The initial and steady-state friction coefficients and the maximum and minimum values for each sample were determined and averaged to characterize the friction properties of the coatings (see Table 6).

**Table 6.** Overview of the friction tests (Ball material—100Cr6, Total distance 5000 cycles or 100 m, Linear velocity 0.15 m/s, Test force—3 N).

	Friction Coefficient			
	NSC 1.1	NSC 1.2	NSC 1.3	Average (NSC 1)
Initial	0.15	0.2	0.17	0.18
Steady-state	0.17	0.2	0.16	
max	0.25	0.61	0.3	
min	0.12	0.08	0.08	
	NSC 2.1	NSC 2.2	NSC 2.3	Average (NSC 2)
Initial	0.32	0.33	0.43	0.72
Steady-state	0.72	0.78	0.64	
max	0.93	1.11	1.04	
min	0.24	0.15	0.16	
	NSC 3.1	NSC 3.2	NSC 3.3	Average (NSC 3)
Initial	0.23	0.26	0.27	0.35
Steady-state	0.34	0.38	0.33	
max	0.85	0.78	1.07	
min	0.1	0.14	0.12	
	Substrate			
Initial	0.56			
Steady-state	0.75			
max	1.01			
min	0.46			

Steady-state coefficients of friction are further used to compare the friction properties of the Coatings. They were calculated from the data obtained in sections of stable value curves containing at least 1000 cycles or 20 m. Examples of friction coefficient curves from each coating and substrate material are summarized in Figure 5. Data were recorded every 0.012 s, and exponential smoothening of the data with a damping factor of 0.8 were performed.

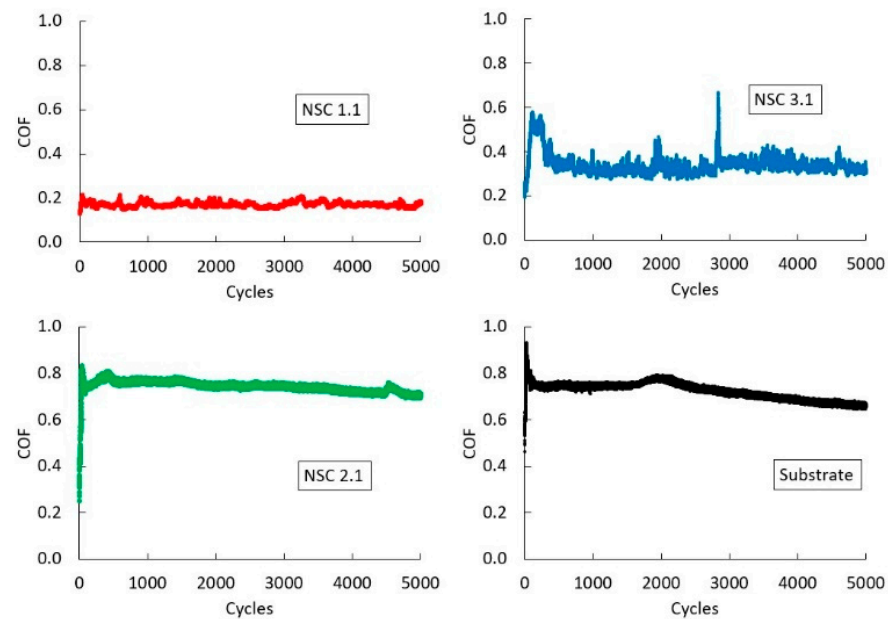


**Figure 5.** Friction coefficient curves for each coating. NSC 1.1—red, NSC 2.1—green, NSC 3.1—blue, substrate—black. Lowest steady-state friction coefficient—NSC 1. 5000 cycles = 100 m.

According to Table 6, the lowest value of the average steady-state friction coefficient was reached for the NSC 1—0.18. Compared to the average steady-state friction coefficient of the substrate material of 0.75, NSC 1 has a reduction in friction of at least four times. The value of the steady-state friction coefficient for NSC 3 is about two times lower than for the substrate material, but more significant curve fluctuations are observed, which could be due to the relatively large wear of this coating. Although the wear is greater than the other two coatings, it did not wear to the substrate material as observed in the wear experiments (see Figure 4). NSC 2 has no friction improvement over the substrate coating.

### 3.3. Surface Texture Measurements

The surface 3D texture parameters were measured for the smooth surface part, or the surface before the tribology experiments and the surface part after the tribology experiments (tribo-tracks from friction experiments (3 N load and 100 m distance) according to the described methodology above (see Figure 2). The surface texture results of different samples in this paragraph are described only by the parameter Sa (see Table 7 and Figure 6) for visibility and simplicity purposes. All used 31 surface texture values are summarized in Tables A1 and A2 in the Appendix A.

**Table 7.** Sa values for the smooth and tribo-track surface parts of three coatings.

Sa Smooth (nm)	Sa Tribo-Track (nm)	Sa Smooth (nm)	Sa Tribo-Track (nm)	Sa Smooth (nm)	Sa Tribo-Track (nm)	Sa Smooth (nm)	Sa Tribo-Track (nm)
11.3	84.1	8.5	102	10.3	70.2	Average (NSC 1) 10 ± 1.2    85 ± 13	
8	64.4	8.8	77.2	6.4	39.7	Average (NSC 2) 7.7 ± 1    60.4 ± 16	
8.8	80.3	11.9	251	11.1	95.6	Average (NSC 3) 10.6 ± 1.3    142.3 ± 77	

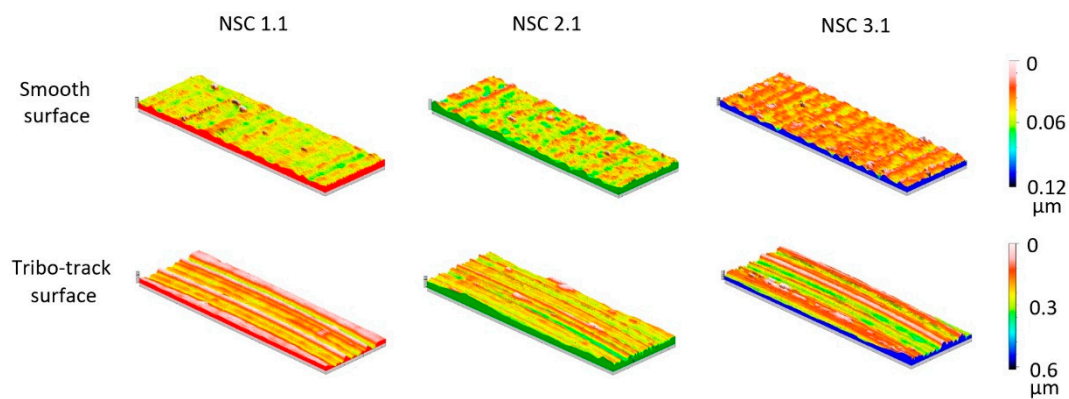


**Figure 6.** Surface texture measurements for smooth and tribo-track surface parts. The scale for a specific surface (smooth or tribo-track) for all three coatings is the same and starts from the highest peak.

If Sa values are compared for the smooth surface, then for the comparison of different coatings, it can be seen that the NSC 1 and NSC 3 coatings have an average Sa value above 10 nm, but the NSC 2 is slightly smoother with an average Sa value around 8 nm. Respectively, for the tribo-track surface, the moderately rougher surface is observed for the NSC 3 coating (Sa 142 nm), the smoothest—for the NSC 2 (Sa 60.4 nm). It should be noted that a significantly rougher surface was observed for NSC 3.2. Therefore, the average value of the Sa tribo-track is also significantly higher. The standard deviation also indicates differences between samples.

Figure 6 represents visual information about the different coating surface textures for the smooth and tribo-track surfaces. The scale values for all three coatings are the same but different for a smooth surface part and tribo-track surface part. For the roughest samples (NSC 3.1) on the tribo-track surface, the roughness has a larger amplitude, which forms a more considerable Sa value. NSC 2.1 has several minor irregularities in amplitude and width compared to NSC 1.1.

### 3.4. Microhardness

Microhardness was measured for each sample in the force range from 0.1 to 6 N (see Table A3 in Appendix A). Each measurement point for each sample consists of 10 measurements, and the average value to represent the hardness of the coating was calculated accordingly. Figure 7 shows the dependence of microhardness values on the applied force when measuring three coatings and substrate material. Examples of visual microscopic images for microhardness measurements at a force of 0.3 N are shown in the second part of the image—a more significant imprint refers to lower hardness.

From Figure 7, it can be concluded that by reducing the applied measurement force, the hardness values increase, but as the load increases, the measured hardness values converge with the hardness of the substrate. As the load decreases, the hardness of the coating directly approaches the hardness of the coating, not the integrated hardness (Coating + Substrate). The indentation depth at 0.1 N was measured to be approximately 0.5  $\mu\text{m}$ , which does not exceed the recommended 10% of coating thickness (ranging from 5.2 to 6.5  $\mu\text{m}$ ) [43]; thus, the microhardness values at 0.1 N force should be close to actual coating hardness. If the coatings are thinner or softer actual coating hardness using Micro-indenter might be problematic to measure. In this case, either mathematical calculations [44] or equipment that provides lower measurement force, such as nano-indenter, should be used.

The highest coating hardness at 0.1 N was obtained for NSC 2 (HV 1710) and NSC 3 (HV 1658), and the lowest for NSC 1 (HV 1507). Compared to the substrate material (HV 967), the hardness increased from 1.6 to 1.8 times.

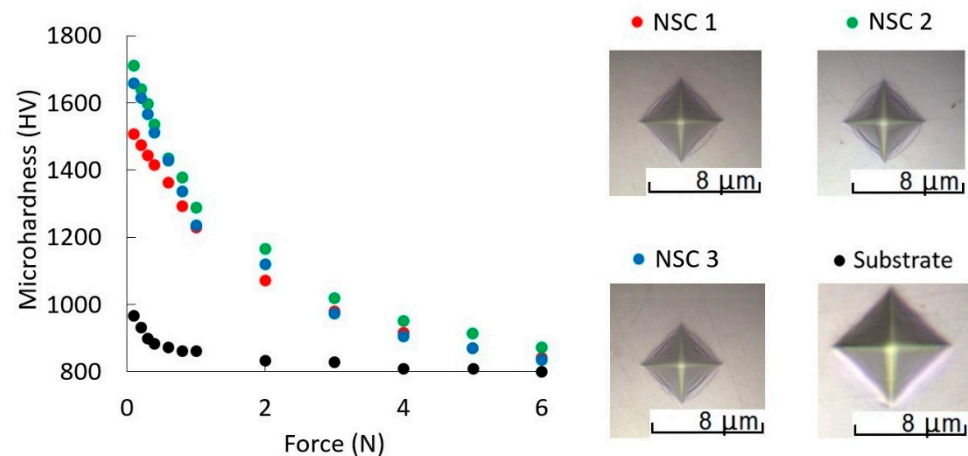


**Figure 7.** Microhardness dependence on indentation force. NSC 1—red, NSC 2—green, NSC 3—blue, substrate—black. As the indentation force decreases, the microhardness increases, respectively. Standard deviation values for calculated measurement points are in the boundaries of the points. The coating imprints from samples NSC 1.1, NSC 2.1, NSC 3.1, and substrate at 0.3 N force are displayed.

### 3.5. Correlation Dependence between Surface Texture and Coating Tribological, Mechanical Properties

As shown by several authors, there is a correlation between the parameters characterizing the surface texture of the sample and the friction coefficient [21,23,24], as well as the coating's hardness [21–23]. Therefore, the correlation between surface texture, friction coefficient, and microhardness was considered for the experimental samples. It has been proven in the known literature [22] that there is a correlation between surface texture parameters and wear; however, with the samples used in the experiments, which have a low surface roughness ( $S_a$  below 12 nm), it was not possible to obtain reliable data confirming the correlation between surface texture and wear. For example, in Dzierwa et al. [22], it was obtained that the surface texture parameter  $S_{sk}$  affects the wear volume. The value of  $S_a$  for all samples was 4  $\mu\text{m}$ . Shi et al. [29], studying how surface texture parameters affect wear, already in the title, emphasizes that the research was carried out on rough surfaces ( $S_a$  from 0.9 to 3.8  $\mu\text{m}$ ). It was found that the void volume parameters affect the wear under hydrodynamic friction conditions; as they increase, the lubricant can penetrate more easily, and thus the surface wear decreases. Perhaps if the surface were rougher, as in other experiments of a similar type, it would be possible to identify the correlation, although, in tests by Sedlacek et al. [39], it was stated that under dry friction regime because of completely changed surface roughness parameters, it is hard to conclude tribological behaviour.

The surface texture measurements and friction coefficient and hardness measurements indicated differences between theoretically three identical samples for each coating; thus, the correlation between the tribological and mechanical properties of the samples and the 3D parameters characterizing the surface texture was considered. The correlation was determined using a correlation coefficient. An example of how the correlation coefficient was determined for each coating is shown in Figure 8. The example uses the correlation of the surface texture parameter  $S_a$  for three samples with a friction coefficient of NSC 1.

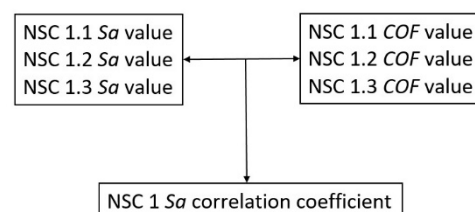


**Figure 8.** Example of correlation coefficient calculation. Three theoretically identical samples (NSC 1.1, NSC 1.2, and NSC 1.3) represent each Coating (NSC 1).



The steady-state friction coefficient was used to characterize friction tests and to identify correlation with surface texture parameters. Microhardness measurements at 0.1 N force (the lowest possible load of the equipment) were used to find the correlation between the surface texture parameters and the microhardness. Therefore, there is reason to believe that surface texture's effect on the coating's hardness under this force would be most probable.

### 3.5.1. Correlation Dependence between Friction Coefficient and Surface Texture

The correlation between friction properties and 3D surface texture parameters was initially sought using the initial friction coefficient and sample surface parameters from smooth surface measurements. However, the results obtained were considered inconsistent, i.e., opposite correlations were observed between the three samples for different coating types. Sedlacek et al. [39] mentioned that under dry sliding, a high degree of wear and changes in surface texture limits a proper comparison and correlation between surface texture and tribological properties; thus alternative method was sought.

Considering the results of inconsistent measurements between the initial friction coefficient and the surface texture of the samples, the correlation between the steady-state friction coefficient and the surface texture parameters of the tribo-track was determined to obtain consistent results. Each sample's steady-state friction coefficient values are represented in Table 6, and considered 3D surface texture parameters are compiled in Table A2 in the Appendix A.

Figure 9 summarizes the TOP 10 highest correlation coefficients for the surface texture parameters of the samples against the steady-state friction coefficient for each Coating (NSC 1—red, NSC 2—green, NSC 3—blue), where each coating includes three samples. A complete graph of the correlation coefficients (including all 31 parameters used) is shown in Figure A1 in Appendix A. Filled bars represent positive correlations, and strikethrough bars—are negative.

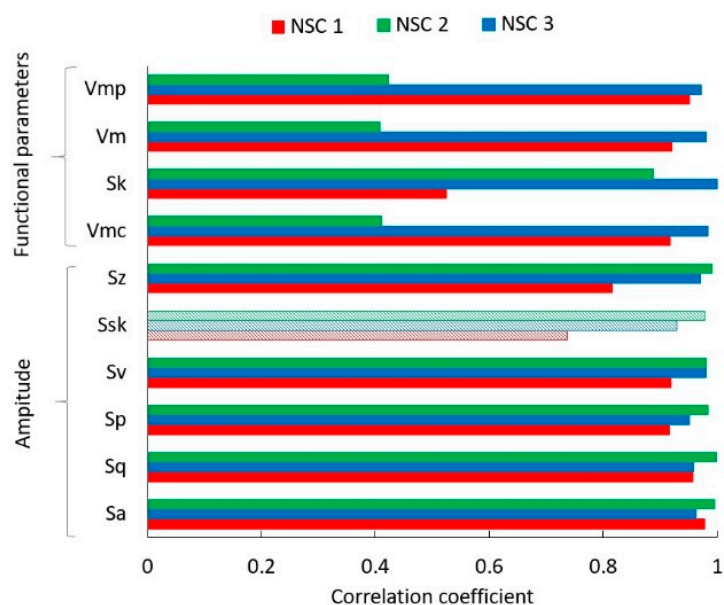


**Figure 9.** Friction coefficient correlation with tribo-track surface roughness parameters (TOP 10). NSC 1—red, NSC 2—green, and NSC 3—blue. Filled bars—positive correlation, strikethrough—negative. Two 3D surface texture parameter groups crystallize—Amplitude and Functional.

It can be seen from Figure 9 that two groups of surface texture parameters crystallize—amplitude and functional parameters, which are related to the material ratio curve. Amplitude parameters such as Sa, Sq, Sz, Sp, and Sv have been reported in previous studies [23,24,26,29,38] as parameters affecting surface contact and friction. Therefore, it is

reasonable to assume that even in the case of nanostructured superlattice coatings, these parameters can be considered primarily. However, it should be noted that the surface texture was measured at the tribo-track location and not on the smooth surface. Ssk (Skewness) is the ratio of the average cube value of the surface ordinates to the cube of the Sq parameter [23]. Therefore, considering that the parameter Ssk is directly dependent on the parameter Sq, the correlation coefficients were also high. In most cases, parameter Ssk was negative, pointing to the surface with the predominance of valley structures. Moreover, Ssk helps monitor different types of wear conditions [41]; therefore, it is logical that this parameter can be successfully used to analyze the correlation with the friction coefficient using surface texture measurements in the tribo-track location. Sedlacek et al. [39] indicated that Ssk is the most dominant parameter affecting friction at the boundary or lubricated conditions, experimenting with ground and polished samples of different surface roughness.

Parameters such as Vmp, Vmc, and Sk have been described in previous studies as parameters affecting wear and friction [23]. Vmp is the peak material volume, representing the volume of material comprising the surface from the height corresponding to a material ratio level p to the highest peak [41]. In this case, the default p-value of 10% of the highest point was used in the measurements. The surface's core height characterizes Sk or core roughness with the predominant peaks and valleys removed. In the future, these correlations should be considered cautious when analyzing the surface at different levels. In this case, the functional parameters were calculated using default material ratios of 10 and 80%. Moreover, compared with the amplitude parameter group, the correlations of functional parameters are not so unambiguous; for example, in the case of Vmp, Vm, and Vmc, correlations below 0.5 were observed for the NSC 2 sample.

Hybrid and spatial surface texture parameter groups showed low correlations for different coatings observed in opposite directions. Considering that isotropic surfaces with the same character were studied, it is impossible to observe sufficient spatial parameter changes between the samples, resulting in correlations in opposite directions. In future studies, the number of samples will be increased; therefore, it is possible that a high correlation could be observed for other 3D surface parameters as well, such as the hybrid parameters Sdr and Sdq, which are affected by both surface texture amplitude and spacing, and can also be successfully used in surface contact, friction and wear characterization [23,25].

### 3.5.2. Correlation Dependence between Microhardness and Surface Texture

The correlation between the microhardness of the coated samples and the surface texture parameters for the smooth surface (see Table A1 in the Appendix A) was determined at a force of 0.1 N (see the microhardness values in Table A3 in the Appendix A). The force was chosen as the lowest technologically possible for the particular equipment Micro-Vickers indenter HM210D (Mitutoyo, Kawasaki, Japan). The penetration depth of the indenter was measured up to approximately 0.5  $\mu\text{m}$ , which exceeds the maximum surface height Sz of the studied samples; therefore, the surface irregularities affect the measurement results indirectly.

Figure 10 summarizes the TOP 10 highest correlation coefficients for the surface texture parameters of the samples against the microhardness values at 0.1 N for each Coating (NSC 1—red, NSC 2—green, NSC 3—blue), where each coating includes three samples. A complete graph of the correlation coefficients is shown in Figure A2 in Appendix A.

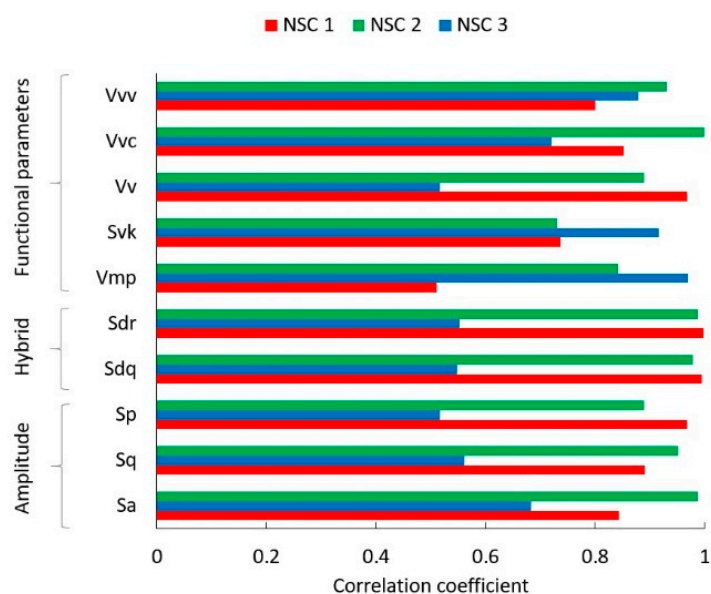


**Figure 10.** Microhardness correlation with smooth surface roughness parameters (TOP 10). NSC 1—red, NSC 2—green, and NSC 3—blue. Filled bars—positive correlation, strikethrough—negative.

From the Figure 10 data, it can be concluded that, similarly to the friction coefficient, high correlations have been obtained with the parameters related to the material ratio curve and amplitude parameters Sa, Sq, Sp. It was observed that the hybrid parameters Sdr and Sdq also correlate well. The surface texture parameter Sdq is highly dependent on the Sq parameter, while the Sdr parameter is dependent on the Sdq parameter [23]; thus, the correlations for the hybrid parameters are also high.

However, the correlation bars indicate that a rougher surface results in higher microhardness, which contradicts previous studies such as Kulej et al. [32] work which described the surface texture and nanohardness of Cu/Ni multilayer structures and obtained that lower Ra (profile roughness height) provides higher hardness. Opposite results were obtained by Bohme et al. [30], where polished surfaces (Ra 2–3 nm) and milled surfaces with traces of machining (Ra 126–240 nm) were produced. The hardness reached 5.7 GPa for the post-polished surface and 7.2 GPa for the machined surface. The error of measurement results for machined surfaces was observed above 40%. Bohme emphasized that it is essential to characterize the surface directly at the indentation point because when indenting at the peak, the material appears softer; when measured in the valley, it appears harder.

Considering obtained results, an additional experiment was performed, creating three surfaces of different roughness on one rectangular sample with dimensions— $30 \times 9 \times 7.5$  mm and material—100Cr6. The sample was polished to Sa 0.04  $\mu\text{m}$ , part of the sample was scratched with 1500 grit sandpaper to Sa 0.06  $\mu\text{m}$ , and another part of the sample was scratched with 600 grit sandpaper to Sa 0.1  $\mu\text{m}$  (see Figure 11). Surface texture measurements were made with the same 3D profilometer and settings as for the samples discussed above.

Microhardness measurements were performed with a Micro-Vickers indenter HM210D (Mitutoyo, Kawasaki, Japan), using 0.2, 0.3, and 0.5 N indentation force. A higher measurement force than in previous experiments was used because the surface roughness is higher than the investigated nano-coated samples, and so the indentations can be analyzed with a contact type 3D profilometer Talysurf Intra 50 (Taylor Hobson, Leicester, UK).

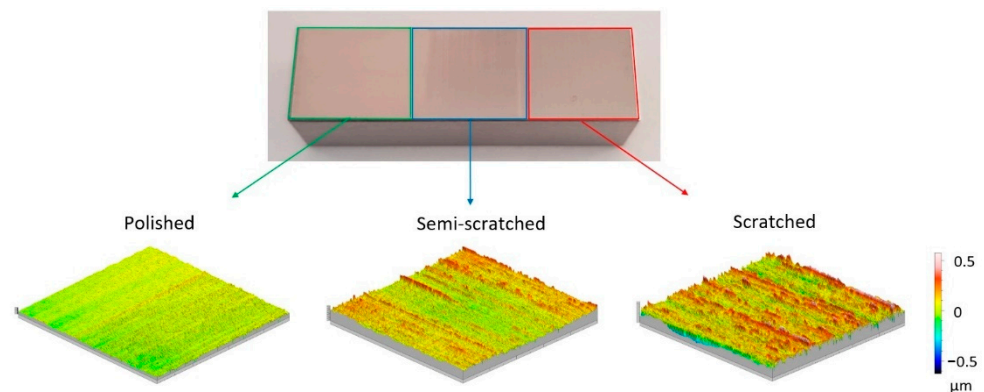


**Figure 11.** 100Cr6 sample with different surface roughness. The green area represents the polished part (Sa 0.04  $\mu\text{m}$ ), the blue—semi-scratched (Sa 0.06  $\mu\text{m}$ ), red—scratched part (Sa 0.1  $\mu\text{m}$ ). The scale bar used is the same for all three surfaces.

The obtained microhardness measurement results can be seen in Figure 12. Each measurement point is calculated as the average of 15 measurements. Unexpectedly, the lowest hardness values were obtained for the polished sample, reaching a difference with the scratched ones of about 40 HV. Moreover, the standard deviations for scratched and semi-scratched surface parts are higher than for polished. That indicates that the measurement error for rougher surfaces tends to be higher, as observed by Bohme [30]. The result agrees with Bohme et al. but is the opposite of what Kulej et al. observed.

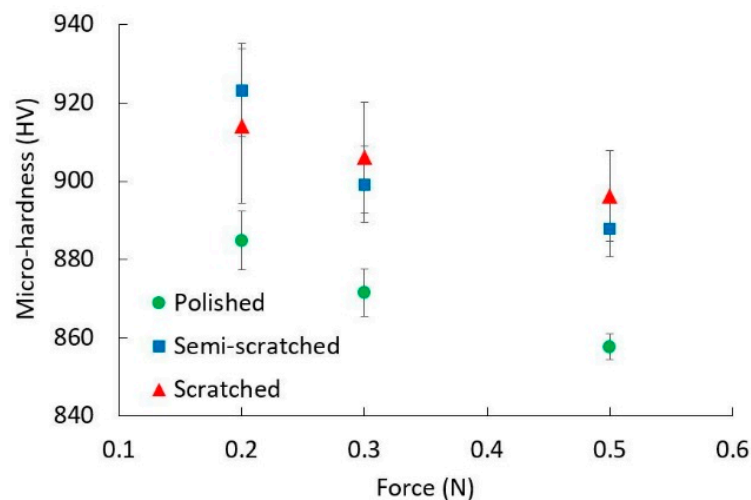


**Figure 12.** Microhardness measurements for three 100Cr6 surface textures. Polished (Sa 0.04  $\mu\text{m}$ )—green, Semi-scratched—blue (Sa 0.06  $\mu\text{m}$ ), Scratched—red (Sa 0.1  $\mu\text{m}$ ).

After the microhardness measurements, a 3D measurement of the surface texture of the indentations was performed (see Figure 13). A 2D profile was cut from the surface measurement midway through the indentation and perpendicular to the machining marks for all three surfaces. In the graph, the left measurement limit (measurement start position) for all three surfaces is defined as the reference limit, and the profiles are arranged accordingly. The arrows indicate the approximate length of measured indentation diagonals. According to the profile data, it can be seen that the limits of indentation measurements can be clearly defined for a polished surface (green profile), but for the scratched and also semi-scratched sample, the measurement limit is more challenging to define because surface roughness prevents it from being accurately determined. It can even be seen that, most likely, the measurement limits for the scratched and semi-scratched surfaces indicate a smaller length of the indentation profile along the X-axis than it is for the polished surface.

Considering the obtained information, it can be concluded that surface texture quality is critically important when performing hardness measurements with a visual reading of measurements.

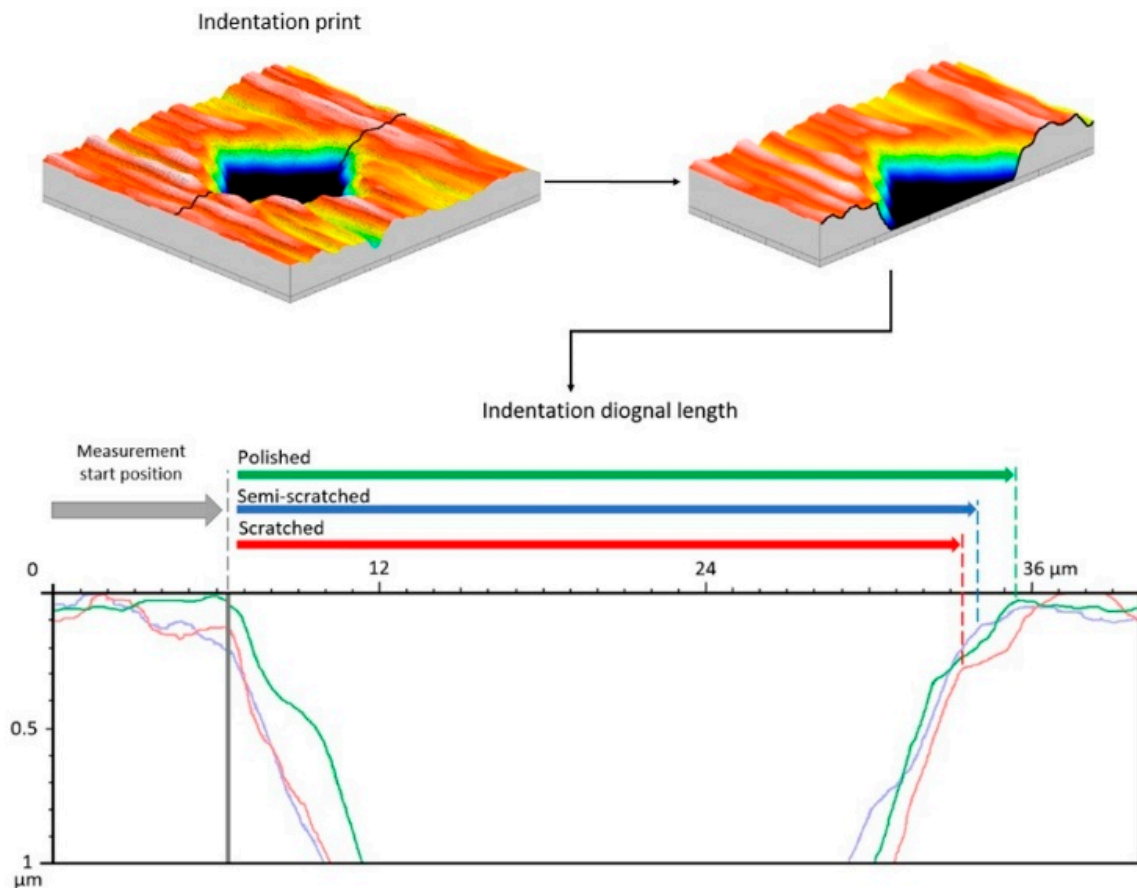


**Figure 13.** Indentation measurements along the X-axis. Profile comparison from measured indentation print at 0.3 N indentation force (thresholded to 1-micrometer depth). Polished ( $S_a$  0.04  $\mu\text{m}$ )—green, Semi-scratched—blue ( $S_a$  0.06  $\mu\text{m}$ ), Scratched—red ( $S_a$  0.1  $\mu\text{m}$ ).

In the case of Nano-coated samples, although seemingly logical parameters related to surface volume and amplitude correlate with surface hardness, the differences in surface roughness are too small to find a reliable relationship between hardness and surface texture. Such a study could be developed with surfaces of markedly different roughness, as demonstrated in an additional study above. However, if the hardness is measured by a visual measurement method, the subjective assumption of the operator when determining the indentation limits has a significant impact on the processing of the measurement data, especially if the surface roughness is high. Similar to the classic hardness indentation, where the hardness is measured depending on the displacement [45], the impact of the surface texture on the hardness measurement results can be observed using the visual microhardness measurement method. As the surface roughness increases, the accuracy of microhardness measurements decreases.

### 3.6. Procedure for Measuring and Evaluating the Surface Texture, Tribological and Mechanical Properties of Deposited Nanocoating

The proposed measurement procedure is intended to analyze nanocoatings and is created based on a holistic approach using three different coatings deposited on a 100Cr6 substrate. The schematic representation of the measurement procedure in Figure 14 and the description below contain the proposed main steps to measure and evaluate nanocoatings.



The principles for developing the surface texture measurement procedure were based on the ISO 10012 standard recommendations. A clause 7.2.2 (Measurement process design) provides the set of guidelines that were taken into account when specifying the measurement processes. Before the measurement procedure was designed, the following elements were considered—necessary measurements, the methods of measurement, and the required equipment for measurements. All three essential elements have been incorporated into the scheme as horizontal dimensions covering the entire measurement process. More specific and detailed information on applied methods is described in the relevant paragraphs of this paper.

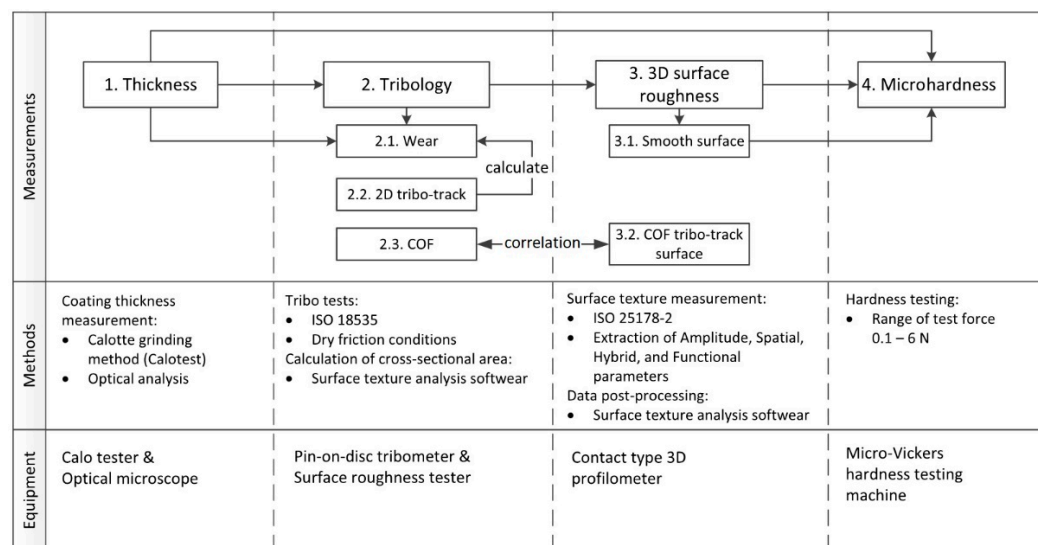


**Figure 14.** Scheme for measuring and evaluating deposited nanocoatings’ surface texture, tribological and mechanical properties.

Initially, it is necessary to determine the thickness of the coating, which can be performed with the standard Calo-tester and an optical microscope. Knowing the thickness of the coating can then evaluate the wear properties of the coating, as well as analyze the microhardness measurements.

Tribology experiments are performed for friction coefficient and wear measurements according to the settings recommended in the ISO 18535 standard. The friction coefficient measurements determine friction properties; the wear measurements determine the coating’s durability. Wear can be measured using a 2D profilometer, obtaining the cross-sectional area or/and calculating the total wear. The recommended number of profiles starts from four at a constant angular distance.

The 3D surface texture measurement is performed for the smooth surface part and the tribo-track part of the friction coefficient. Three-dimensional surface texture measurement provides more accurate and complete information about the surface. The measurement of the smooth part allows to estimate of the surface texture of the coating and can also be used for further analysis of the surface microhardness. The tribo-track surface texture measurement of the friction coefficient showed a high correlation with the steady-state friction coefficient values, which makes it possible to analyze the relationship between the friction coefficient and the surface texture. In this case, the texture of the smooth surface did not show significant differences between the different samples, so no correlation was established.

Microhardness measurements are recommended to be performed in the broadest possible indentation force range, thereby determining the integrated hardness (Coating + Substrate) for each sample.

The developed procedure for measuring and evaluating nanocoatings systematically collects the most important information about the surface, tribological, and mechanical

properties. The procedure will be further improved and refined by performing more measurements with different nanocoatings. One of the recommended measures to improve the procedure would be to define what skills are required for the personnel performing the measurements, as defined in the ISO 10012 standard. As the measurements for this study were carried out in a scientific laboratory by qualified scientific personnel, the skills set for the personnel were not included in this procedure.

#### 4. Conclusions

The above-noted general empirical formula for modified non-stoichiometric NSC based on  $\{\text{TiMe}_1\text{Me}_2\text{-CN/TiAlSi-N}\}_n$  where 'Me<sub>1</sub> and Me<sub>2</sub>' denote alloying metallic additives as, e.g., Cr, Nb, W, and Zr but subscript 'n' indicates a number of periods within the NSC containing alternating {carbonitride/nitride} sublayers includes numerous modifications of metal-based carbonitride/nitride multilayered ceramic coatings manifesting high wear resistance (up to 28 times against substrate material), low friction coefficient (up to four times against substrate material) and high surface hardness (up to 1.6 times against substrate material).

Microhardness measurements in the applied force range from 0.1 to 6.0 N allow the integrated hardness changes to be evaluated depending on the applied force. As the applied indentation force increases, the impact of the coating on the result of the microhardness measurement decreases. At 6.0 N applied force, the measured microhardness values of the coated samples start to converge with the microhardness value of the substrate (the difference is less than 8%).

The surface roughness significantly impacts the results using the visual microhardness measurement method. As the roughness increases, the accuracy of microhardness measurements decreases. The standard deviation decreased approximately two times as applied force increased from 0.2 to 0.5 N, and the standard deviation was almost three times higher for the rougher surface (Sa 0.1 μm) compared to the polished one (Sa 0.04 μm).

High correlation dependence between the steady-state friction coefficient and the amplitude (correlation coefficient above 0.8 in 94% of cases) and functional (correlation coefficient above 0.8 in 67% of cases) surface texture parameters of the tribo-track surface were obtained.

Based on a holistic approach, a procedure for measuring and evaluating nanocoatings was developed at the initial stage, allowing systematic coatings analysis.

**Author Contributions:** Conceptualization E.J., J.L. and I.B.; methodology J.L., E.J., A.L., U.K. and I.B.; investigation A.L., J.L., E.J., U.K. and K.K.; writing—original draft preparation E.J.; writing—review and editing E.J., J.L., U.K., O.L., G.C. and I.B.; visualization E.J., J.L. and G.C.; supervision I.B.; project administration I.B. and G.C.; funding acquisition I.B. All authors have read and agreed to the published version of the manuscript.

**Funding:** This research is funded by the Latvian Council of Science, project "Carbon-rich self-healing multifunctional nanostructured smart coatings (NSC) for high-tech applications using high-power confined plasma technology for their deposition", project No. 2019/1-0385.

**Data Availability Statement:** Not applicable.

**Acknowledgments:** The authors express gratitude to Mitutoyo Poland Sp.o.o. for providing the Microhardness measurement equipment used in this study.

**Conflicts of Interest:** The authors declare no conflict of interest.

## Appendix A

Table A1. Surface Texture measurements (smooth part).

Parameter	NSC 1				NSC 2				NSC 3			
	NSC 1.1	NSC 1.2	NSC 1.3	Avg.	NSC 2.1	NSC 2.2	NSC 2.3	Avg.	NSC 3.1	NSC 3.2	NSC 3.3	Avg.
Sa (nm)	11.3	8.5	10.3	10.0	8.8	11.9	11.1	10.6	8	8.8	6.4	7.7
Sq (nm)	16.9	12.1	15.6	14.9	14.2	22.5	19.2	18.6	11.1	11.9	8.4	10.5
Sp (nm)	120	80.7	118	106	109	208	164	160.3	66.9	68.7	38.3	58.0
Sv (nm)	46.2	34.4	34.5	38.4	26.8	36.7	52.9	38.8	29.9	25.7	21.7	25.8
Ssk	1.9	1.5	2.4	1.9	3.4	5.1	3.7	4.1	1.2	0.9	0.4	0.8
Sku	15.5	12.9	19.0	15.8	24.4	42.7	31.2	32.8	9.8	7.2	4.5	7.2
Sz (nm)	164	114	151	143	135	242	214	197	96	93	59	83
RSm (mm)	0.008	0.007	0.008	0.008	0.009	0.019	0.011	0.013	0.006	0.006	0.007	0.006
RSm/Sa	699	825	748	757	994	1580	991	1188	780	722	1059	854
Sq/Sa	1.5	1.4	1.5	1.5	1.6	1.9	1.7	1.7	1.4	1.4	1.3	1.4
Sp/Sz	0.73	0.71	0.78	0.74	0.81	0.86	0.77	0.81	0.70	0.74	0.65	0.70
Sds (pks/mm <sup>2</sup> )	9621	10,171	10,312	10,035	11,233	9230	10,369	10,277	11,657	10,173	11,473	11,101
Str	0.44	0.44	0.41	0.43	0.30	0.50	0.39	0.40	0.55	0.67	0.36	0.53
Sal (mm)	$4.10 \times 10^{-4}$	$4.10 \times 10^{-4}$	$3.90 \times 10^{-4}$	$4.03 \times 10^{-4}$	$2.80 \times 10^{-4}$	$4.70 \times 10^{-4}$	$3.70 \times 10^{-4}$	$3.73 \times 10^{-4}$	$3.90 \times 10^{-4}$	$4.70 \times 10^{-4}$	$2.60 \times 10^{-4}$	$3.73 \times 10^{-4}$
Sfd	2.44	2.48	2.44	2.45	2.38	2.30	2.30	2.33	2.54	2.58	2.62	2.58
Sdq	0.015	0.014	0.016	0.015	0.015	0.018	0.017	0.017	0.013	0.014	0.011	0.013
Ssc (1/ $\mu$ m)	0.033	0.034	0.035	0.034	0.029	0.041	0.036	0.035	0.030	0.037	0.027	0.031
Sdr (%)	0.012	0.010	0.012	0.011	0.011	0.016	0.014	0.014	0.009	0.010	0.006	0.008
Sk (nm)	25.3	20.4	22.6	22.8	19.7	24.4	22.8	22.3	19.2	21.9	15.8	19.0
Spk	24.1	15.9	23.1	21.0	25.4	41.6	33.1	33.4	14.3	14.6	8.5	12.5
Svk	15.6	10.5	13.0	13.0	9.0	14.5	15.6	13.0	10.1	9.3	6.5	8.6
Sr1	12.1	10.4	11.8	11.4	11.4	11.9	11.4	11.6	10.8	10.6	10.5	10.6
Vv	$1.20 \times 10^{-4}$	$8.08 \times 10^{-5}$	$1.18 \times 10^{-4}$	$1.06 \times 10^{-4}$	$1.09 \times 10^{-4}$	$2.08 \times 10^{-4}$	$1.64 \times 10^{-4}$	$1.60 \times 10^{-4}$	$6.69 \times 10^{-5}$	$6.87 \times 10^{-5}$	$3.84 \times 10^{-5}$	$5.80 \times 10^{-5}$
Vm	$4.60 \times 10^{-5}$	$3.38 \times 10^{-5}$	$3.41 \times 10^{-5}$	$3.80 \times 10^{-5}$	$2.60 \times 10^{-5}$	$3.60 \times 10^{-5}$	$5.20 \times 10^{-5}$	$3.80 \times 10^{-5}$	$2.95 \times 10^{-5}$	$2.53 \times 10^{-5}$	$2.14 \times 10^{-5}$	$2.54 \times 10^{-5}$
Vmp	$7.00 \times 10^{-6}$	$5.29 \times 10^{-6}$	$5.75 \times 10^{-6}$	$6.01 \times 10^{-6}$	$5.00 \times 10^{-6}$	$7.07 \times 10^{-6}$	$8.16 \times 10^{-6}$	$6.74 \times 10^{-6}$	$4.60 \times 10^{-6}$	$4.54 \times 10^{-6}$	$3.50 \times 10^{-6}$	$4.21 \times 10^{-6}$
Vmc	$3.30 \times 10^{-5}$	$2.47 \times 10^{-5}$	$2.51 \times 10^{-5}$	$2.76 \times 10^{-5}$	$1.90 \times 10^{-5}$	$2.56 \times 10^{-5}$	$3.75 \times 10^{-5}$	$2.74 \times 10^{-5}$	$2.18 \times 10^{-5}$	$1.87 \times 10^{-5}$	$1.58 \times 10^{-5}$	$1.88 \times 10^{-5}$
Vvc	$1.60 \times 10^{-5}$	$1.20 \times 10^{-5}$	$1.45 \times 10^{-5}$	$1.42 \times 10^{-5}$	$1.20 \times 10^{-5}$	$1.50 \times 10^{-5}$	$1.44 \times 10^{-5}$	$1.38 \times 10^{-5}$	$1.15 \times 10^{-5}$	$1.31 \times 10^{-5}$	$9.59 \times 10^{-6}$	$1.14 \times 10^{-5}$
Vvv	$2.00 \times 10^{-5}$	$1.32 \times 10^{-6}$	$1.62 \times 10^{-6}$	$1.65 \times 10^{-6}$	$1.00 \times 10^{-6}$	$1.70 \times 10^{-6}$	$1.75 \times 10^{-6}$	$1.48 \times 10^{-6}$	$1.30 \times 10^{-6}$	$1.31 \times 10^{-6}$	$9.41 \times 10^{-7}$	$1.18 \times 10^{-6}$
Spk/Sk	0.95	0.78	1.02	0.92	1.29	1.7	1.45	1.48	0.74	0.67	0.54	0.65
Svk/Sk	0.62	0.51	0.58	0.57	0.46	0.59	0.68	0.58	0.53	0.42	0.41	0.45
Spk/Svk	1.54	1.51	1.78	1.61	2.81	2.87	2.12	2.60	1.42	1.57	1.31	1.43

Table A2. Surface Texture measurements (tribo-track part).

Parameter	NSC 1			NSC 2			NSC 3					
	NSC 1.1	NSC 1.2	NSC 1.3	NSC 1.1	NSC 1.2	NSC 1.3	NSC 1.1	NSC 1.2	NSC 1.3	NSC 1.1	NSC 1.2	NSC 1.3
Sa (nm)	84	102	70	85	80	251	96	142	64	77	40	60
Sq (nm)	100	117	82	100	99	326	124	183	87	108	54	83
Sp (nm)	221	262	156	213	241	1114	359	571	256	351	188	265
Sv (nm)	254	325	143	241	255	1860	260	792	345	482	252	360
Ssk	−0.6	−0.6	0.0	−0.4	−0.1	−1.3	1.2	−0.1	−0.4	−0.6	0.3	−0.2
Sku	2.7	2.0	2.0	2.2	2.8	5.9	3.8	4.2	4.7	5.1	4.9	4.9
Sz (nm)	460	500	297	419	493	2600	620	1238	600	813	424	612
RSm (mm)	0.009	0.016	0.015	0.013	0.014	0.020	0.013	0.016	0.011	0.011	0.009	0.010
RSm/Sa	107	157	214	159	174	80	136	130	171	143	227	180
Sq/Sa	1.2	1.1	1.2	1.2	1.2	1.3	1.3	1.3	1.4	1.4	1.4	1.4
Sp/Sz	0.5	0.5	0.5	0.5	0.5	0.4	0.6	0.5	0.4	0.4	0.4	0.4
Sds (pks/mm <sup>2</sup> )	5526	10,559	4409	6831	10,682	5898	6870	7817	9623	8486	8616	8908
Str	0.04	0.08	0.03	0.05	0.04	0.04	0.04	0.04	0.04	0.04	0.15	0.07
Sal (mm)	$4.57 \times 10^{-4}$	$7.39 \times 10^{-4}$	$3.25 \times 10^{-4}$	$5.07 \times 10^{-4}$	$5.53 \times 10^{-4}$	$4.73 \times 10^{-4}$	$3.59 \times 10^{-1}$	$1.20 \times 10^{-1}$	$1.75 \times 10^{-4}$	$2.82 \times 10^{-4}$	$3.20 \times 10^{-4}$	$2.59 \times 10^{-4}$
Sfd	2.08	2.20	2.11	2.13	2.18	2.12	2.10	2.13	2.15	2.16	2.16	2.16
Sdq	0.03	0.03	0.02	0.03	0.05	0.09	0.04	0.06	0.06	0.06	0.03	0.05
Ssc (1/μm)	0.29	0.23	0.22	0.25	0.22	0.38	0.36	0.32	0.31	0.23	0.14	0.23
Sdr (%)	0.05	0.03	0.03	0.04	0.12	0.42	0.08	0.21	0.16	0.16	0.06	0.13
Sk (nm)	226	204	127	186	218	443	171	277	227	222	101	183
Spk	72	128	119	106	82	145	232	153	76	117	65	86
Svk	63	31	48	47	93	599	95	262	122	196	59	126
Sr1	17.2	21.6	17.9	18.9	10.1	5.4	18.9	11.5	7.0	9.9	8.7	8.5
Vv	$2.21 \times 10^{-7}$	$2.01 \times 10^{-7}$	$1.56 \times 10^{-7}$	$1.93 \times 10^{-7}$	$2.41 \times 10^{-4}$	$8.05 \times 10^{-4}$	$3.60 \times 10^{-4}$	$4.69 \times 10^{-4}$	$2.57 \times 10^{-7}$	$3.51 \times 10^{-4}$	$1.88 \times 10^{-4}$	$1.80 \times 10^{-4}$
Vm	$2.52 \times 10^{-7}$	$3.24 \times 10^{-7}$	$1.41 \times 10^{-7}$	$2.39 \times 10^{-7}$	$2.54 \times 10^{-4}$	$1.86 \times 10^{-3}$	$2.57 \times 10^{-4}$	$7.90 \times 10^{-4}$	$3.43 \times 10^{-7}$	$4.80 \times 10^{-4}$	$2.49 \times 10^{-4}$	$2.43 \times 10^{-4}$
Vmp	$3.67 \times 10^{-8}$	$4.70 \times 10^{-8}$	$2.52 \times 10^{-8}$	$3.63 \times 10^{-8}$	$4.10 \times 10^{-5}$	$2.23 \times 10^{-4}$	$5.02 \times 10^{-5}$	$1.05 \times 10^{-4}$	$4.69 \times 10^{-8}$	$6.38 \times 10^{-5}$	$3.22 \times 10^{-5}$	$3.20 \times 10^{-5}$
Vmc	$1.96 \times 10^{-7}$	$2.51 \times 10^{-7}$	$1.10 \times 10^{-7}$	$1.86 \times 10^{-7}$	$1.90 \times 10^{-4}$	$1.35 \times 10^{-3}$	$1.79 \times 10^{-4}$	$5.73 \times 10^{-4}$	$2.52 \times 10^{-7}$	$3.51 \times 10^{-4}$	$1.81 \times 10^{-4}$	$1.77 \times 10^{-4}$
Vvc	$1.01 \times 10^{-7}$	$1.16 \times 10^{-7}$	$1.03 \times 10^{-7}$	$1.07 \times 10^{-7}$	$1.15 \times 10^{-4}$	$3.04 \times 10^{-4}$	$2.02 \times 10^{-4}$	$2.07 \times 10^{-4}$	$8.91 \times 10^{-8}$	$1.01 \times 10^{-4}$	$5.41 \times 10^{-5}$	$5.17 \times 10^{-5}$
Vvv	$1.30 \times 10^{-8}$	$9.91 \times 10^{-9}$	$7.86 \times 10^{-9}$	$1.03 \times 10^{-8}$	$1.12 \times 10^{-5}$	$4.98 \times 10^{-5}$	$7.04 \times 10^{-6}$	$2.27 \times 10^{-5}$	$1.32 \times 10^{-8}$	$1.82 \times 10^{-5}$	$6.76 \times 10^{-6}$	$8.32 \times 10^{-6}$
Spk/Sk	0.32	0.63	0.94	0.63	0.38	0.33	1.36	0.69	0.33	0.53	0.64	0.50
Svk/Sk	0.28	0.15	0.38	0.27	0.43	1.35	0.56	0.78	0.54	0.88	0.59	0.67
Spk/Svk	1.15	4.08	2.48	2.57	0.88	0.24	2.44	1.19	0.62	0.60	1.10	0.77

Table A3. Microhardness measurement values.

	Test Force (N)	NSC 1.1 (HV)	NSC 1.2 (HV)	NSC 1.3 (HV)	Average (HV)		Test Force (N)	NSC 3.1 (HV)	NSC 3.2 (HV)	NSC 3.3 (HV)	Average (HV)
NSC 1	6	854	837	831	841	NSC 3	6	842	843	819	835
	5	883	866	860	870		5	871	884	852	869
	4	935	916	897	916		4	904	932	876	904
	3	1000	986	951	979		3	963	1013	941	972
	2	1118	1094	1002	1071		2	1075	1257	1025	1119
	1	1189	1255	1245	1230		1	1210	1292	1204	1235
	0.8	1244	1315	1321	1293		0.8	1294	1378	1334	1335
	0.6	1338	1345	1405	1363		0.6	1402	1455	1425	1427
	0.4	1406	1356	1483	1415		0.4	1519	1546	1472	1512
	0.3	1448	1366	1514	1443		0.3	1575	1608	1515	1566
	0.2	1491	1366	1564	1474		0.2	1618	1660	1562	1613
0.1	1550	1370	1602	1507	0.1	1658	1715	1602	1658		
	Test Force (N)	NSC 2.1 (HV)	NSC 2.2 (HV)	NSC 2.3 (HV)	Average (HV)		Test force (N)	Substr. (HV)		Average (HV)	
NSC 2	6	882	898	835	872	Substrate	6	800			800
	5	931	927	881	913		5	794			794
	4	967	965	920	951		4	809			809
	3	1055	1028	977	1020		3	828			828
	2	1191	1188	1116	1165		2	833			833
	1	1278	1289	1300	1289		1	861			861
	0.8	1379	1356	1401	1379		0.8	862			862
	0.6	1424	1413	1470	1436		0.6	872			872
	0.4	1515	1510	1583	1536		0.4	883			883
	0.3	1584	1574	1636	1598		0.3	898			898
	0.2	1632	1625	1664	1640		0.2	931			931
0.1	1667	1708	1756	1710	0.1	967			967		



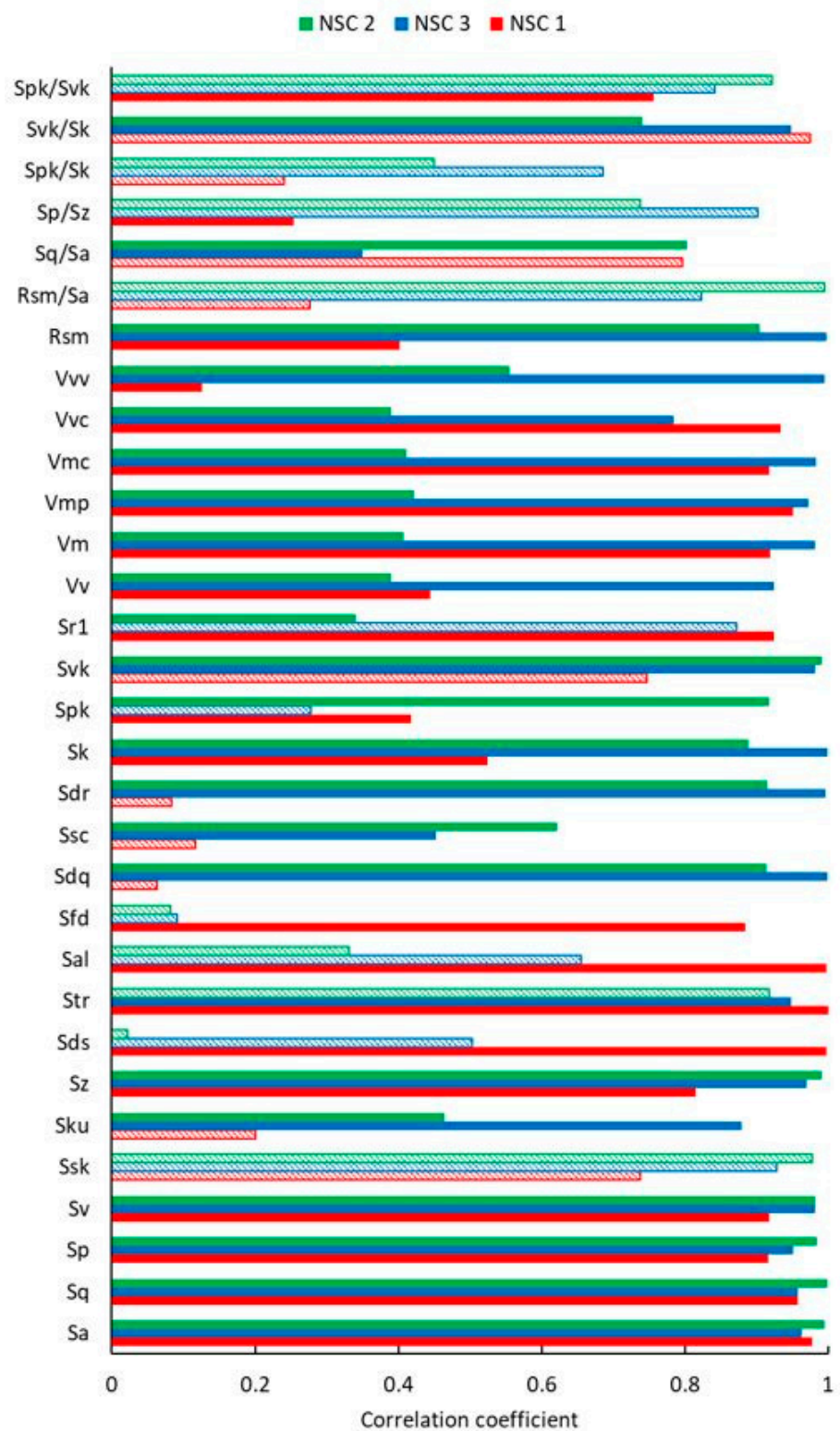


Figure A1. Friction coefficient correlation with tribo-track surface texture.

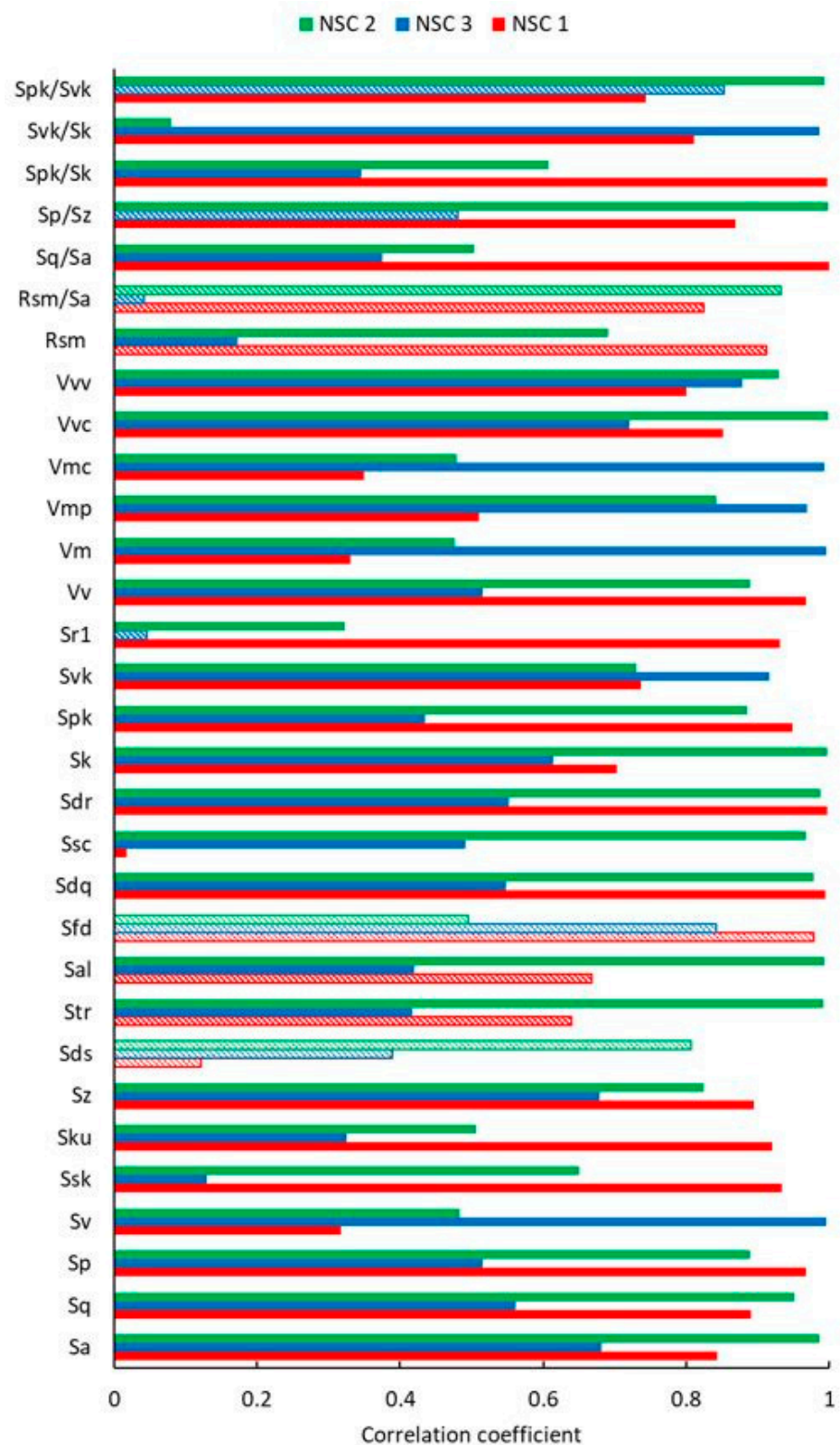


Figure A2. Microhardness correlation with smooth surface texture.

## References

1. Kassfeldt, E.; Lundmark, J. Tribological Properties of Hardened High Strength Boron Steel at Combined Rolling and Sliding Condition. *Wear* **2009**, *267*, 2287–2293. [[CrossRef](#)]
2. Tryba, D.; Kot, M.; Antosz, A. An Analysis of Wear and Mechanical and Tribological Properties of High-Manganese Steel Hardened by Different Methods. *Q. Tribol.* **2018**, *280*, 137–142. [[CrossRef](#)]

3. Rakhadilov, B.; Seitkhanova, A.; Satbayeva, Z.; Yerbolatova, G.; Icheva, Y.; Sagdoldina, Z. Investigation of the Structural, Mechanical and Tribological Properties of Plasma Electrolytic Hardened Chromium-Nickel Steel. *Lubricants* **2021**, *9*, 108. [[CrossRef](#)]
4. Borges, F.C.N.; de Oliveira, W.R.; Kublitski, J. Mechanical, Structural and Tribological Properties of Superaustenitic Stainless Steel Submitted at Solution Heat Treatment. *Matéria* **2015**, *20*, 160–168. [[CrossRef](#)]
5. Owens, A.G.; Brühl, S.; Simison, S.; Forsich, C.; Heim, D. Comparison of Tribological Properties of Stainless Steel with Hard and Soft DLC Coatings. *Procedia Mater. Sci.* **2015**, *9*, 246–253. [[CrossRef](#)]
6. Komarov, F.F.; Konstantinov, V.M.; Kovalchuk, A.V.; Konstantinov, S.V.; Tkachenko, H.A. The effect of steel substrate pre-hardening on structural, mechanical, and tribological properties of magnetron sputtered TiN and TiAlN coatings. *Wear* **2016**, *352–353*, 92–101. [[CrossRef](#)]
7. He, Q.; DePaiva, J.M.; Kohlscheen, J.; Veldhuis, S.C. A study of mechanical and tribological properties as well as wear performance of a multifunctional bilayer AlTiN PVD coating during the ultra-high-speed turning of 304 austenitic stainless steel. *Surf. Coat. Technol.* **2021**, *423*, 127577. [[CrossRef](#)]
8. Zhang, H.; Mei, F.; Yu, Y.; Lin, X.; Gao, J. Improvement on the mechanical, tribological properties and cutting performance of AlTiN-based coatings by compositional and structural design. *Surf. Coat. Technol.* **2021**, *422*, 127503. [[CrossRef](#)]
9. Joshi, M.; Adak, B. Advances in Nanotechnology Based Functional, Smart and Intelligent Textiles: A Review. *Compr. Nanosci. Nanotechnol.* **2019**, *1–5*, 253–290. [[CrossRef](#)]
10. Wu, W.Y.; Ting, J.M. Growth and characteristics of metal-containing diamond-like carbon using a self-assembled process. *Carbon N. Y.* **2006**, *44*, 1210–1217. [[CrossRef](#)]
11. Persson, K.; Gåhlin, R. Tribological performance of a DLC coating in combination with water-based lubricants. *Tribol. Int.* **2003**, *36*, 851–855. [[CrossRef](#)]
12. Chang, Y.Y.; Lai, H.M. Wear behavior and cutting performance of CrAlSiN and TiAlSiN hard coatings on cemented carbide cutting tools for Ti alloys. *Surf. Coat. Technol.* **2014**, *259*, 152–158. [[CrossRef](#)]
13. Miletić, A.; Panjan, P.; Škorić, B.; Čekada, M.; Dražič, G.; Kovač, J. Microstructure and mechanical properties of nanostructured Ti–Al–Si–N coatings deposited by magnetron sputtering. *Surf. Coat. Technol.* **2014**, *241*, 105–111. [[CrossRef](#)]
14. Chen, H.; Zheng, B.C.; Li, Y.G.; Wu, Z.L.; Lei, M.K. Flexible hard TiAlSiN nanocomposite coatings deposited by modulated pulsed power magnetron sputtering with controllable peak power. *Thin Solid Film.* **2019**, *669*, 377–386. [[CrossRef](#)]
15. Münz, W.D.; Donohue, L.A.; Hovsepian, P.E. Properties of various large-scale fabricated TiAlN- and CrN-based superlattice coatings grown by combined cathodic arc–unbalanced magnetron sputter deposition. *Surf. Coat. Technol.* **2000**, *125*, 269–277. [[CrossRef](#)]
16. Hovsepian, P.E.; Lewis, D.B.; Müunz, W.D.; Rouzaud, A.; Juliet, P. Chromium nitride/niobium nitride superlattice coatings deposited by combined cathodic-arc/unbalanced magnetron technique. *Surf. Coat. Technol.* **1999**, *116–119*, 727–734. [[CrossRef](#)]
17. Wang, T.; Xie, L.-J.; Wang, X.-B.; Shang, T.-Y. 2D and 3D milled surface roughness of high volume fraction SiCp/Al composites. *Def. Technol.* **2015**, *11*, 104–109. [[CrossRef](#)]
18. Deleanu, L.; Georgescu, C.; Suciuc, C. A Comparison between 2D and 3D Surface Parameters for Evaluating the Quality of Surfaces. *Ann. Dunarea Jos Univ. Galati Fascicle V Technol. Mach.* **2012**, *30*, 5–12.
19. Librera, E.; Riva, G.; Safarzadeh, H.; Previtali, B. On the use of areal roughness parameters to assess surface quality in laser cutting of stainless steel with CO<sub>2</sub> and fiber sources. *Procedia CIRP* **2015**, *33*, 532–537. [[CrossRef](#)]
20. Zawada-Tomkiewicz, A. Analysis of surface roughness parameters achieved by hard turning with the use of PCBN tools. *Est. J. Eng.* **2011**, *17*, 88–99. [[CrossRef](#)]
21. Menezes, P.L.; Kishore; Kailas, S.V.; Lovell, M.R. Role of surface texture, roughness, and hardness on friction during unidirectional sliding. *Tribol. Lett.* **2011**, *41*, 1–15. [[CrossRef](#)]
22. Dzierwa, A. Effects of Surface Preparation on Friction and Wear in Dry Sliding Conditions. *Q. Tribol.* **2017**, *272*, 25–31. [[CrossRef](#)]
23. Pawlus, P.; Reizer, R.; Wieczorowski, M. Functional Importance of Surface Texture Parameters. *Materials* **2021**, *14*, 5326. [[CrossRef](#)] [[PubMed](#)]
24. Kacalak, W.; Lipiński, D.; Róžański, R.; Królczyk, G.M. Assessment of the classification ability of parameters characterizing surface topography formed in manufacturing and operation processes. *Measurement* **2021**, *170*, 108715. [[CrossRef](#)]
25. Żak, K.; Grzesik, W. Metrological aspects of surface topographies produced by different machining operations regarding their potential functionality. *Metrol. Meas. Syst.* **2017**, *24*, 325–335. [[CrossRef](#)]
26. Das, J.; Linke, B. Evaluation and systematic selection of significant multi-scale surface roughness parameters (SRPs) as process monitoring index. *J. Mater. Process. Technol.* **2017**, *244*, 157–165. [[CrossRef](#)]
27. Zeng, Q.; Qin, Y.; Chang, W.; Luo, X. Correlating and evaluating the functionality-related properties with surface texture parameters and specific characteristics of machined components. *Int. J. Mech. Sci.* **2018**, *149*, 62–72. [[CrossRef](#)]
28. Jansons, E.; Lungevics, J.; Gross, K.A. Surface roughness measure that best correlates to ease of sliding. In Proceedings of the Engineering for Rural Development, Jelgava, Latvia, 25–27 May 2016.
29. Shi, R.; Wang, B.; Yan, Z.; Wang, Z.; Dong, L. Effect of Surface Topography Parameters on Friction and Wear of Random Rough Surface. *Materials* **2019**, *12*, 2762. [[CrossRef](#)]

30. Böhme, L.; Keksel, A.; Ströer, F.; Bohley, M.; Kieren-Ehse, S.; Kirsch, B.; Aurich, J.C.; Seewig, J.; Kersch, E. Micro hardness determination on a rough surface by using combined indentation and topography measurements. *Surf. Topogr. Metrol. Prop.* **2019**, *7*, 045021. [[CrossRef](#)]
31. Plichta, T.; Zahradnicek, R.; Cech, V. Surface topography affects the nanoindentation data. *Thin Solid Film.* **2022**, *745*, 139105. [[CrossRef](#)]
32. Kulej, E.; Kucharska, B.; Pyka, G.; Gwoździk, M. Characterization of the surface topography and nano-hardness of Cu/Ni multilayer structures. *Cent. Eur. J. Phys.* **2011**, *9*, 1421–1425. [[CrossRef](#)]
33. Maniks, J.; Mitin, V.; Kanders, U.; Kovalenko, V.; Nazarovs, P.; Baitimirova, M.; Meija, R.; Zabels, R.; Kundzins, K.; Erts, D. Deformation behavior and interfacial sliding in carbon/copper nanocomposite films deposited by high power DC magnetron sputtering. *Surf. Coat. Technol.* **2015**, *276*, 279–285. [[CrossRef](#)]
34. Leitans, A.; Lungevics, J.; Kanders, U.; Boiko, I. Micromechanical and Tribological Properties of Nanostructured Carbonitride Coatings Deposited by PVD Technique. *Key Eng. Mater.* **2021**, *903*, 177–182. [[CrossRef](#)]
35. Shiryaev, S.A.; Atamanov, M.V.; Guseva, M.I.; Martynenko, Y.V.; Mitin, A.V.; Mitin, V.S.; Moskovkin, P.G. Production and properties of metal-carbon composite coatings with a nanocrystalline structure. *Tech. Phys.* **2002**, *47*, 238–243. [[CrossRef](#)]
36. Mitin, V.S.; Sharipov, E.I.; Mitin, A.V. High deposition rate magnetrons: Key elements and advantages. *Surf. Eng.* **2013**, *22*, 5–10. [[CrossRef](#)]
37. Wang, B.; Zheng, M.; Zhang, W. Analysis and Prediction of Wear Performance of Different Topography Surface. *Materials* **2020**, *13*, 5056. [[CrossRef](#)]
38. Deltombe, R.; Kubiak, K.J.; Bigerelle, M. How to select the most relevant 3D roughness parameters of a surface. *Scanning* **2014**, *36*, 150–160. [[CrossRef](#)]
39. Sedlaček, M.; Gregorčič, P.; Podgornik, B. Use of the Roughness Parameters Ssk and Sku to Control Friction—A Method for Designing Surface Texturing. *Tribol. Trans.* **2016**, *60*, 260–266. [[CrossRef](#)]
40. Linins, O.; Jansons, E.; Leitans, A.; Boiko, I.; Lungevics, J. Estimation of Service Life of Mechanical Engineering Components. *Key Eng. Mater.* **2019**, *799*, 71–76. [[CrossRef](#)]
41. Michigan Metrology. *Surface Texture Parameters Glossary*; Michigan Metrology LLC: Livonia, MI, USA, 2014.
42. Li, Z.; Wang, J.; Zhang, H.; Chen, J.; Liu, K. Influence of surface topography on the friction and dynamic characteristics of spur gears. *J. Eng. Tribol.* **2020**, *234*, 1892–1907. [[CrossRef](#)]
43. Chen, K.S.; Chen, T.C.; Ou, K.S. Development of semi-empirical formulation for extracting materials properties from nanoindentation measurements: Residual stresses, substrate effect, and creep. *Thin Solid Film.* **2008**, *516*, 1931–1940. [[CrossRef](#)]
44. Wei, Z.; Zhang, G.; Chen, H.; Luo, J.; Liu, R.; Guo, S. A simple method for evaluating elastic modulus of thin films by nanoindentation. *J. Mater. Res.* **2009**, *24*, 801–815. [[CrossRef](#)]
45. Oliver, W.C.; Pharr, G.M. Measurement of hardness and elastic modulus by instrumented indentation: Advances in understanding and refinements to methodology. *J. Mater. Res.* **2004**, *19*, 3–20. [[CrossRef](#)]